2021

CHARACTERIZING THE SEASONAL AND ENVIRONMENTAL EFFECTS ON HIGH FREQUENCY ACOUSTIC FISH TAG DETECTION IN SHALLOW WATER SETTINGS

Jacob Bonney
University of Rhode Island, jakebonney10@uri.edu

CHARACTERIZING THE SEASONAL AND ENVIRONMENTAL EFFECTS ON HIGH FREQUENCY ACOUSTIC FISH TAG DETECTION IN SHALLOW WATER SETTINGS

BY

JACOB BONNEY

A THESIS SUBMITTED IN PARTIAL FULFILLMENT OF THE REQUIREMENTS FOR THE DEGREE OF

MASTER OF SCIENCE

IN

OCEAN ENGINEERING

UNIVERSITY OF RHODE ISLAND

2021

MASTER OF SCIENCE IN

OCEAN ENGINEERING THESIS

OF

JACOB BONNEY

APPROVED:

Thesis Committee:

Major Professor James H. Miller

Gopu R. Potty

Conor McManus

Eric Schneider

Brenton DeBoef
DEAN OF THE GRADUATE SCHOOL

UNIVERSITY OF RHODE ISLAND
2021

ABSTRACT

Networks of high frequency (69kHz) acoustic fish tracking tags and receiver arrays are commonly used by marine biologists and fisheries management programs to determine the spatial and temporal distribution of a marine species. Despite the widespread use of these networks for monitoring fish movement ecology, there is often limited information to inform suitable receiver array spacing for optimal detection probability, or confidence estimates in tag detections. This is further confounded by the effects that seasonal and environmental changes can have on acoustic propagation. To evaluate these effects, the effective range of high frequency acoustic transmitters for medium and large fish (Vemco V16®) was measured in active passive acoustic receiver locations throughout Narragansett Bay under varying environmental and seasonal conditions. The physical factors occurring in the recorded field data were validated using acoustic modeling techniques, showing that receiver array spacing for any location can be determined through simulation if the environmental characteristics of the acoustics soundscape are known, thereby mitigating the need for rigorous and expensive field testing to determine tag detection ranges for this system. Receiver detection data was used in a logistic regression generalized linear model to estimate probability of detection with range and to inform a detection a threshold level at 50% detectability. The detection threshold was set where modeled results reached a level of 8 dB above recorded noise levels and modeled results using Bellhop yielded detection ranges between 688.7 - 878.8 meters for the Narragansett Bay range testing

sites. Several hypothetical modeling scenarios which examined the effect of changing individual acoustic environmental characteristics other than noise, revealed that decreased detection ranges were associated with seafloor attenuation characteristics, especially in downward refracting environments (summer thermoclines). Changes in detection range due to varying receiver depth were found to be minimal in shallow water locations (20-60 meters), however they were more substantial in deeper water locations with significant thermoclines (150+ meters). Conversely, model scenarios with tags and receivers located below thermoclines exhibited increased detection ranges across all seasons. In summer months, seafloors comprised of silty sediments had detection ranges far lower than scenarios with a sandy seafloor. When considering receiver array construction, these results reveal that caution should be taken when placing receiver arrays near the sea surface, and that bottom sediment type should also be accounted for, as environments with silty sediments will experience greater loss than those with sandy seafloors. Additionally, receiver array spacing should be adjusted during summer months to account for additional transmission loss due to downward refracting rays and increased bottom losses.

ACKNOWLEDGMENTS

I would like to thank my major advisor, Dr. James Miller for his constant support and mentorship throughout the years. Your door was always open, and I never hesitated to walk in and ask for advice. You have a way of keeping things lighthearted and friendly while delivering critical and constructive criticism, and I've appreciated that. I'd also like to thank Dr. Gopu Potty for always providing expert insight throughout every one of our meetings and discussions. Great appreciation goes to the team at RIDEM DMF, especially the other members of my thesis committee, Dr. Conor McManus, and Eric Schneider. I am so appreciative of the patience and commitment you've had helping me reach my research goals. Whether it was coordinating ship time, securing research gear and equipment for field tests, or providing critical insight into the biology and fisheries aspect of this project, your support made this project possible. To Heather Stoffel of the URI GSO's Marine Ecosystems Research Laboratory (MERL), thank you for continuously supporting our equipment needs and CTD data collection. Without your equipment much of our field work wouldn't have been possible. Much appreciation also extends to undergraduate Research Assistant Peter Maranan, who on a moment's notice was willing to participate in days long field work deployments, acoustic modeling efforts, and any task I needed extra assistance on. And finally, a special thank you goes out to my best friend Angela Quagliaroli. I owe the world to you, my family, and all my friends for your never-ending support of my goals and dreams.

TABLE OF CONTENTS

LIST OF TABLES

LIST OF FIGURES

CHAPTER 1

INTRODUCTION

In recent years, coastal tagging programs, consisting of acoustic fish tags and receivers, have increased in prevalence to monitor fish movement of coastal gateways, rivers, and shorelines along the Atlantic coastline [1]. In many cases, tag data collected by receiver arrays is used by fisheries scientists to understand fish species movement ecology for their conservation and management [2]. With the increasing prevalence of this technology, it becomes increasingly important that users understand the tag detectability uncertainty to both inform the acoustic receiver designs and properly interpret their tagging data. The acoustic fish tag manufacturer Vemco currently recommends a methodology for estimating detectability that does not consider the effects of the acoustic environment. Current detection range estimates are often based on statistical analysis of multi-year static field deployments in receiver areas. This methodology proves both costly and time consuming while also failing to investigate the underlying drivers responsible for changes in the acoustic environment that can affect tag detections (or propagation, etc.).

The work described in this thesis shows an alternative and novel approach for estimating the detection range of high frequency acoustic fish tags. A series of drifts at active receiver locations present within Rhode Island (RI) waters measured the acoustic transmission loss over range for a Vemco V16 69kHz fish

tag. Using environmental characteristics of the acoustic soundscape recorded during testing, the acoustic propagation modeling tool Bellhop [3] was used to model the transmission loss of the Vemco fish tag with range. The modeled output was compared to and validated by the measured acoustic field data showing that transmission loss of high frequency acoustic fish tags can be determined through simulation. A logistic regression model was used to model the binary probability of detection output from Vemco VR2W receivers collected during testing. The modeled transmission loss levels (Bellhop) and probability of detection (GLM) informed the decision to set a level of 8 dB above recorded noise levels as the 50% probability of detection threshold. After determining this threshold, additional environmental scenarios were modeled in Bellhop to illustrate the effects of variation in the acoustic environment on detection range. The results can be used to inform adjustments to receiver array designs, and to quantify the detectability of tagged fishes present within a study area quantify, such as the effectiveness of the array to describe the ingress and egress of species within the region. The following sections within the introduction will provide further information on the project background, and a description of the thesis content.

1.1. Project Background

The work for this thesis was funded through a joint grant awarded to the University of Rhode Island, Department of Ocean Engineering (URI) and Rhode Island Department of Environmental Management Division of Marine Fisheries (RIDEM) to identify the spatial and temporal distribution of Atlantic sturgeon

(*Acipenser oxyrhynchus oxyrhynchus*) in RI state waters [4]. This anadromous species spends most of its life in marine waters but make seasonal migrations to spawning and foraging grounds within estuaries and rivers throughout their latitudinal range (Labrador, Canada to St. Johns River, FL) [5]. Atlantic sturgeon are listed as a federally endangered species within the New York Bight Distinct Population Segment (DPS), which includes Rhode Island state waters, under the US Endangered Species Act. They are also listed in RI as a species of greatest conservation need in the RI State Wildlife Action Plan (SWAP) [6]. To address threats of “fishing impacting population’s sustainability” and “capture as bycatch” listed under the RI SWAP, the grant awarded to URI and RIDEM proposed to assess the movement and population distribution of Atlantic sturgeon in RI waters using acoustic telemetry techniques to monitor Atlantic sturgeon tagged by other institutes along the Atlantic coast. Prior to initiating this project, no hydroacoustic fish tag receivers were present within Rhode Island state waters and the area was one of several no coverage zones in the Atlantic Cooperative Telemetry (ACT) Network [7] (Figure 1). As a part of the ACT Network, more than 1,331 Atlantic Sturgeon outfitted with acoustic tags were detected by arrays of acoustic receivers located in coastal waters on the US east coast between January of 2006 and December of 2015 [8]. Filling in the gaps along the coastal network of receivers in areas such as RI allows for researchers to gain a greater understanding of the overall seasonal and temporal distribution of Atlantic sturgeon. The primary objectives of the RIDEM and URI grant were as follows:

Objective 1: Design, construct, and deploy a series of hydroacoustic receiver arrays to detect Atlantic sturgeon carrying acoustic tags.

Objective 2: *Conduct post-deployment testing to determine the effects of seasonal and environmental aspects on tag detection.*

Objective 3: Use tag return data generated from the arrays to determine the spatial and temporal distribution of Atlantic sturgeon in RI waters.

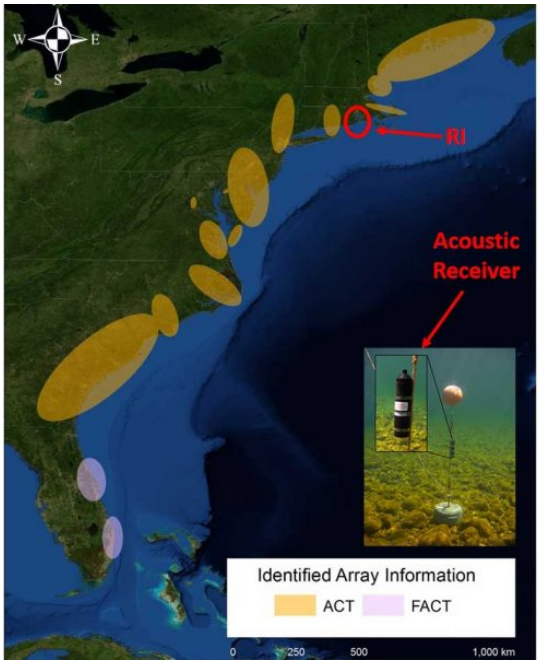

Figure 1: This map portrays the general areas along the Atlantic coast with hydro-acoustic arrays that are part of the ACT network as of 2018. The area depicted with the red circle is the general study area of this project [6].

As of September 2021, there are a total of 28 hydroacoustic receivers deployed within RI state waters, 15 of which are operated by the RIDEM and 13 by the Atlantic Shark Institute (ASI). The design of the acoustic receiver arrays as a part of the RIDEM-URI grant were primarily vertical mooring setups, however some receivers within RI waters have been attached to the hard foundations of physical

structures such as docks or environmental monitoring systems. Moored receivers are fixed to lines approximately 2-3 meters from the seafloor, while deep water locations off the coast of Block Island are surface mounted within 1 meter of the surface (Figure 2).

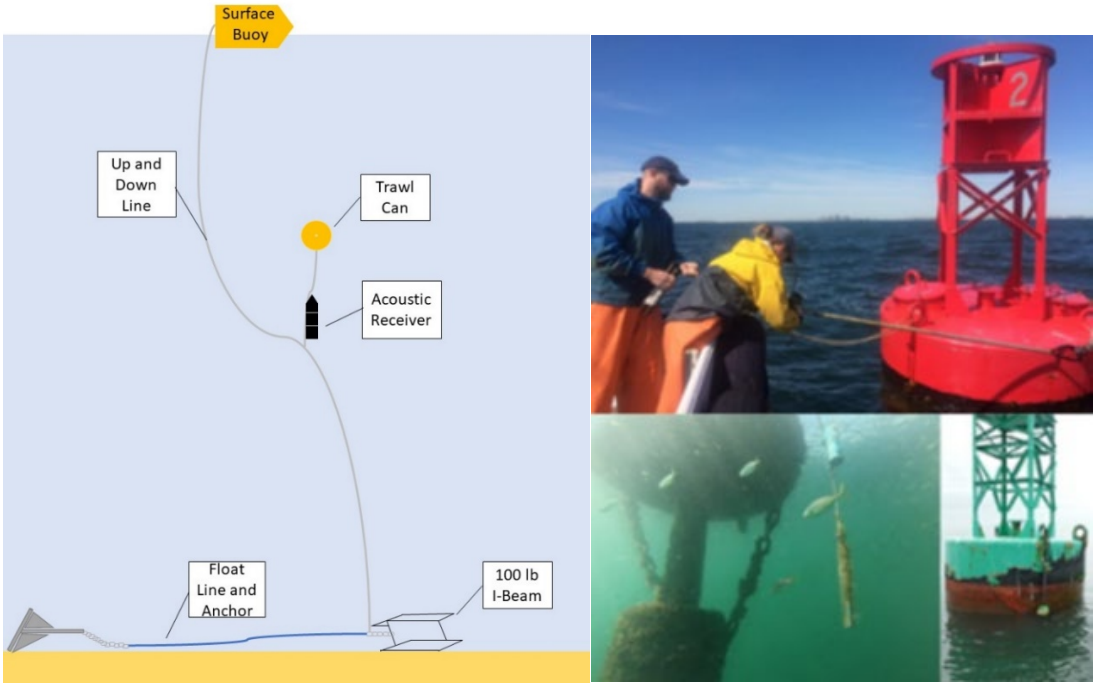

Figure 2: RIDEM vertical receiver array design [9] (left) and an example of receiver's surface mounted to navigation aids.

Array locations (Figure 3) are situated along the south shore of Rhode Island and at the mouth of Narragansett Bay to capture migrating species moving along the coast and in/out of the estuary. Locations South surrounding Block Island are used by ASI to detect white sharks typically found further offshore and receiver locations within RI waters are utilized for capturing directionality of fish traveling up the Bay or along the shoreline. Directionality is determined, for example, when

fish carrying acoustic tags are detected as they enter through a chokepoint at the mouth of Narragansett Bay and continue to travel north where they are detected at a second chokepoint. Data collected at these chokepoints provide insight into the time tagged fish migrate into regions, which direction they are headed, how long they remain in a region, and when they leave. The value of directionality measurements at these chokepoints emphasizes the need for adequate array spacing so there is confidence that all tagged fishes moving through a region are detected. The distancing between receivers located at choke points in the East and West Passages and Sakonnet River have been adjusted periodically to account for detectability estimates determined during post deployment sensitivity testing as a part of Objective 2, the primary focus of this thesis work.

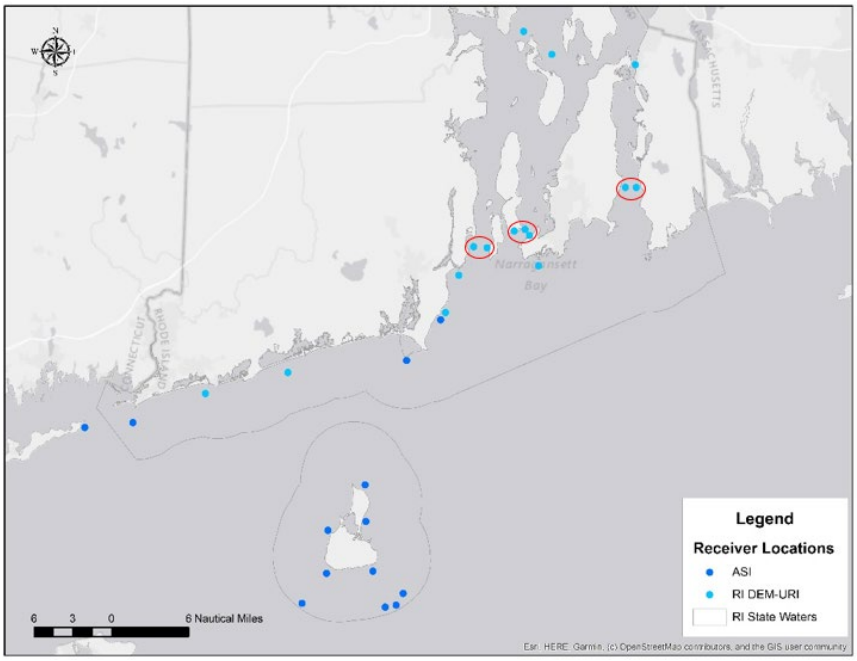

Figure 3: VEMCO VR2W receiver arrays in RI waters. RIDEM/URI Receiver locations listed in light blue. ASI receivers in darker blue. Location of range testing sites for this study circled in red [9].

Objective 3 has been ongoing since the receiver array was constructed. The acoustic telemetry equipment deployed as a part of this grant were Vemco VR2W-69 kHz acoustic monitoring receivers, capable of detecting any animal equipped with a Vemco transmitter. Across the nine receivers deployed during the 2019 and 2020 calendar year, a total of 1,807 acoustic tag detections (Table 1) from 92 unique acoustic tags (Table 2) were recorded. Tagged species detected in RI waters included striped bass, river herring, Atlantic cod, various shark species, and more than 15 tagged fish which have yet to be identified. Tag return data at RIDEM receiver locations has been dominated by striped bass and species more commonly found within RI waters, however several Atlantic sturgeons have also been detected. Since April of 2019 when the first receivers were deployed, five Atlantic sturgeons have been detected a total of 60 times. After retrieving and processing receiver data deployed during the first year of the project, minimal tag return data from the Sakonnet River receiver locations (Table 1) suggested tag detections may be impacted by the array design and the acoustic environment, further justifying the need for post deployment sensitivity testing as described in Objective 2.

Table 1: Number of acoustic tag detections (i.e., pings recorded) from acoustically tagged fish at each station during the Performance Period (Oct 2019 – Sept 2020). Note that a given tag may be detected multiple times; thus, the number of detections is not an indicator of the number of individual fish detected [4].

Station		Acoustic Tag Detections (Pings Recorded)												
		2019			2020									
Number	Name	Oct	Nov	Dec	Jan	Feb	Mar	April	May	Jun	Jul	Aug	Sep	Total
1	Sakonnet East	7	.	.	NA	NA	.	.	.	17	.	.	.	24
2	Sakonnet West	29	.	.	NA	NA	.	.	.	6	.	.	.	35
3	Hammersmith Farm	19	.	.	NA	NA	.	.	51	48	4	.	.	122
4	Kettle Bottom	9	.	.	NA	NA	.	.	41	53	38		7	148
5	Dutch Island	.	.	.	NA	NA	.	.	.	.	.	.	.	0
6	Austin Hollow	.	.	.	NA	NA	.	.	.	8	33			41
7	Rivers Ledge	107	21	.	NA	NA	.	.	17	33	12	29	232	451
8	Ninigret Breachway	106	9	.	NA	NA	NA	NA	22	28	11	1	51	228
9	Weekapaug Point	217	12	.	NA	NA	NA	NA	49	96	93	30	60	557
10	Bonnet Point	.	.	.	NA	NA	.	.	.	53	148	.	.	201
	Total	494	42	0	0	0	0	0	180	342	339	60	350	1807

Table 2: Number of unique acoustic tags detected (i.e., fish) and the number of detections (i.e., pings recorded) per fish species by month during the Performance Period (Oct 2019 – Sept 2020) [4].

	Acoustic Tags	Acoustic Tag Detections (Pings Recorded)												
		2019			2020									
Name	Detected	Oct	Nov	Dec	Jan	Feb	Mar	April	May	Jun	Jul	Aug	Sep	Total
Atlantic cod	1	19	.	.	NA	NA	.	.	.	.	.	.	.	19
Atlantic sturgeon	2	.	.	.	NA	NA	.	.	.	12	.	.	.	12
Blueback herring	1		9	.	NA	NA	.	.	.	.	.	.	.	9
Not Identified	15	10	.	.	NA	NA	.	.	178	242	1	.	.	431
Sand tiger shark	2	10	.	.	NA	NA	.	.	.	17	.	.	10	37
Sandbar shark	1	.	.	.	NA	NA	.	.	.	.	.	1	.	1
Smooth dogfish	1	.	.	.	NA	NA	.	.	.	.	.	15	.	15
Striped bass	69	455	33	.	NA	NA	.	.	2	71	338	44	340	1283
Total	92	494	42	.	.	.	.	.	180	342	339	60	350	1807

1.1. Thesis Content

Chapter 2 consists of a literature review that focuses on acoustic telemetry and detection theory, the research methods and findings of detection range studies, the environmental factors effecting acoustic propagation, and high frequency acoustic modeling using Bellhop. Chapter 3 describes the methods, strategies, and design used in this research project to perform range testing, data processing, and acoustic modeling. Chapter 4 presents the results of this experiment. Finally, Chapter 5 summarizes the major findings and limitations of this approach, potential sources of error, and future considerations for acoustic fish tag range and detectability studies.

List of References

[1] Kraus RT, Holbrook CM, Vandergoot CS, et al. Evaluation of acoustic telemetry grids for determining aquatic animal movement and survival. Methods Ecol Evol. 2018;00:1–14. https://doi.org/10.1111/2041-210X.12996

[2] Bangley, C.W., Whoriskey, F.G., Young, J.M. and Ogburn, M.B. (2020), Networked Animal Telemetry in the Northwest Atlantic and Caribbean Waters. Mar Coast Fish, 12: 339-347. https://doi.org/10.1002/mcf2.10128

[3] Porter, M. (2019). The BELLHOP Manual and User's Guide.

[4] Eric Schneider. Rhode Island Marine Fisheries Institute. U.S. Fish and Wildlife State Wildlife Grant. DOCUMENTING THE SPATIAL AND TEMPORAL DISTRIBUTION OF ATLANTIC STURGEON IN RHODE ISLAND STATE WATERS (uri.edu)

[5] Hilton, E.J., B. Kynard, M.T. Balazik, A.Z. Horodysky, and C.B. Dillman. 2017. Review of the biology, fisheries, and conservation status of the Atlantic sturgeon (Acipenser oxyrinchus oxyrinchus Mitchell, 1815). Journal of Applied Ichthyology 32 (Suppl. 1): 30-66.

[6] Rhode Island Department of Environmental Management (RIDEM). 2015. Rhode Island State Wildlife Action Plan (RI SWAP). Available at: http://www.dem.ri.gov/programs/fish-wildlife/wildlifehuntered/swap15.php

[7] ACT (Atlantic Cooperative Telemetry) Network. 2020. The Atlantic Cooperative Telemetry Network. Available: www.theactnetwork.com. (April 2020).

[8] Atlantic States Marine Fisheries Commission (ASMFC). 2017. Atlantic Sturgeon Benchmark Stock Assessment Report for Peer Review. Stock Asses. Rep. No. XX-XX X. ASMFC, Arlington VA. 237 pp. Manuscript in peer review.

[9] Chris Parkins. Rhode Island Department of Environmental Management Division of Marine Fisheries Acoustic Telemetry Array (RIDEM DMF). 2021.

CHAPTER 2

REVIEW OF LITERATURE

The following sections will review literature about acoustic telemetry and detection theory, notable detection range and probability of detection studies, the environmental factors that affect acoustic propagation, and the Bellhop acoustic propagation model.

2.1. Acoustic Telemetry and Detection Theory

Coded acoustic telemetry devices, such as the Vemco V16 69 kHz tag, use unmodulated, fixed frequency pulses with information coded in the spacing between pulses to transmit and decipher unique serial ID numbers associated with individual tags [1] [2]. This encoding technique is referred to as Pulse Position Modulation (PPM) (Figure 4).

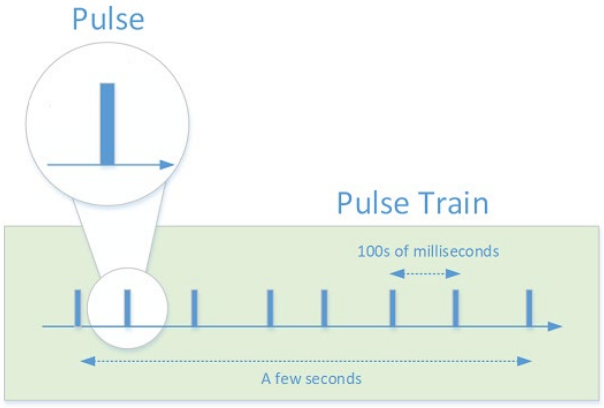

Coding schemes identify the length between ping intervals or number of intervals present, and receivers are configured with a code map to detect all Vemco tags currently present in the field [1]. Randomization of delays between successive transmissions accommodate multiple transmitters being present in each area and decreases the probability of tag collisions [1]. The signal processing methodology used by Vemco Receivers to determine whether a signal is classified as a detection is proprietary, however classic detection theory states that the detection of acoustic signals in any given environment is dependent on the Signal to Noise Ratio (SNR) measured at the output of a receiver [3]. The Neyman Pearson criterion is a widely used strategy for determining whether a signal of interest was detected or not within a subset of data and works by establishing a detection threshold to maximize the probability of detection *p(D),* for a given probability of false alarm *p(FA)* [4].

$$p(D) = p(FA)^{\frac{1}{1+SNR}}$$

Shown in the equation above, the Neyman Pearson criterion can be manipulated to give an expression for SNR that is required to obtain the desired *p(D)* for a given *p(FA)* [5]. There are 4 potential outcomes when detecting a signal (Table 3): null decision, false alarm, miss, and correct decision. A null decision occurs when no signal is present, and the decision is no detection. A false alarm occurs when no signal is present, yet the decision is that there is a detection. A miss occurs when a signal is present, and the decision is no detection. Finally, a correct decision occurs when a signal is present, and the decision is a detection. Consider the three different signal levels, and the two different detection

thresholds set at T_1 and T_2 (Figure 5). With the detection threshold set high at T_1, there will be one correct decision and two misses, however there will be no false alarms. With a lower threshold set at T_2, there will be three correct detections, but there will also be 3 additional false alarms considered as detections. An inverse relationship arises between detection and false alarm probability with decreasing thresholds (Figure 5). Although the Neyman-Pearson criterion may not be used by fish tag manufacturers such as Vemco, it is important to understand relationship between signal level, noise level, and detection thresholds when considering the probability of detection for acoustic transmitters and receivers.

Table 3: Potential outcomes of Neyman Pearson criterion and their effect on the probability of detection and false alarm. Credit DOSITS [5].

		Decision	
		Signal Absent	Signal Present
At receiver input	Signal absent	Null decision 1-p(FA)	False alarm p(FA)
	Signal present	Miss 1-p(D)	Correct Detection p(D)

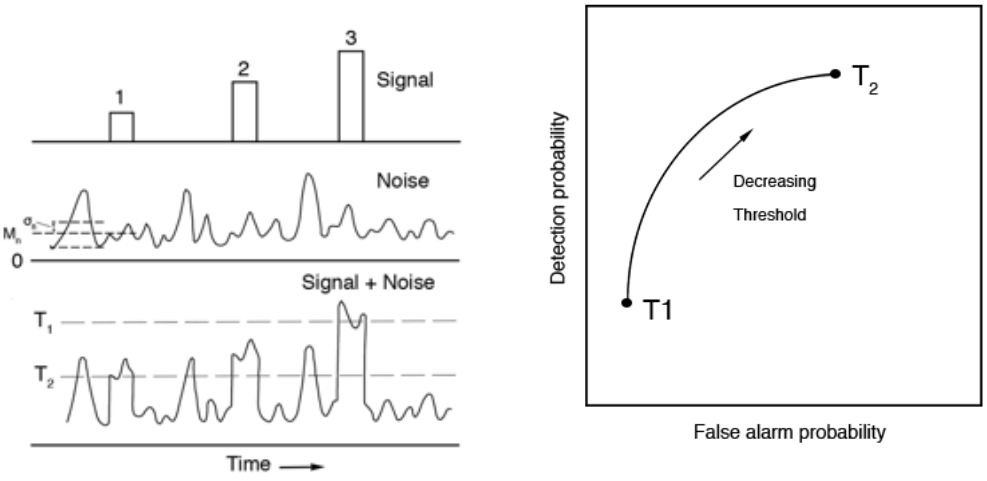

Figure 5: Example (Left) of signal, noise, and SNR threshold levels present in a detection scenario and relationship (Right) between detection and false alarm probability with decreasing SNR threshold. Credit DOSITS [5].

2.2. Detection Range and Probability of Detection Studies

Manufacturers of fish tracking tags typically provide an overly optimistic baseline distance for detection range and array spacing, considering impacts that seasonal and environmental conditions can have on acoustic propagation. For example, the Vemco V16 69 kHz tags are advertised to have a baseline range of several hundred meters and in good conditions between 800-1200 meters [6] [7]. However, Vemco emphasizes the need to perform range testing to determine appropriate receiver spacing and detection range [7]. The techniques commonly used to accomplish this rely on statistical analyses of receiver detections over time [8]. Detection data is collected over a period of days, weeks, months, or years and is analyzed to determine the number detections compared the number of expected detections [8]. Common setup for range testing studies (Figure 6) like those performed by Loher et al [9], require several stationary receiver configurations spaced out at set intervals (e.g., 400, 600, 800, 1000 meters) from range testing tags. While this strategy is effective at formulating probability of detection estimates for a given location and time, it fails to effectively capture the underlying physical phenomena causing episodic periods of decreased tag detection range. Due to this, range testing is recommended for every receiver location present in a study [8].

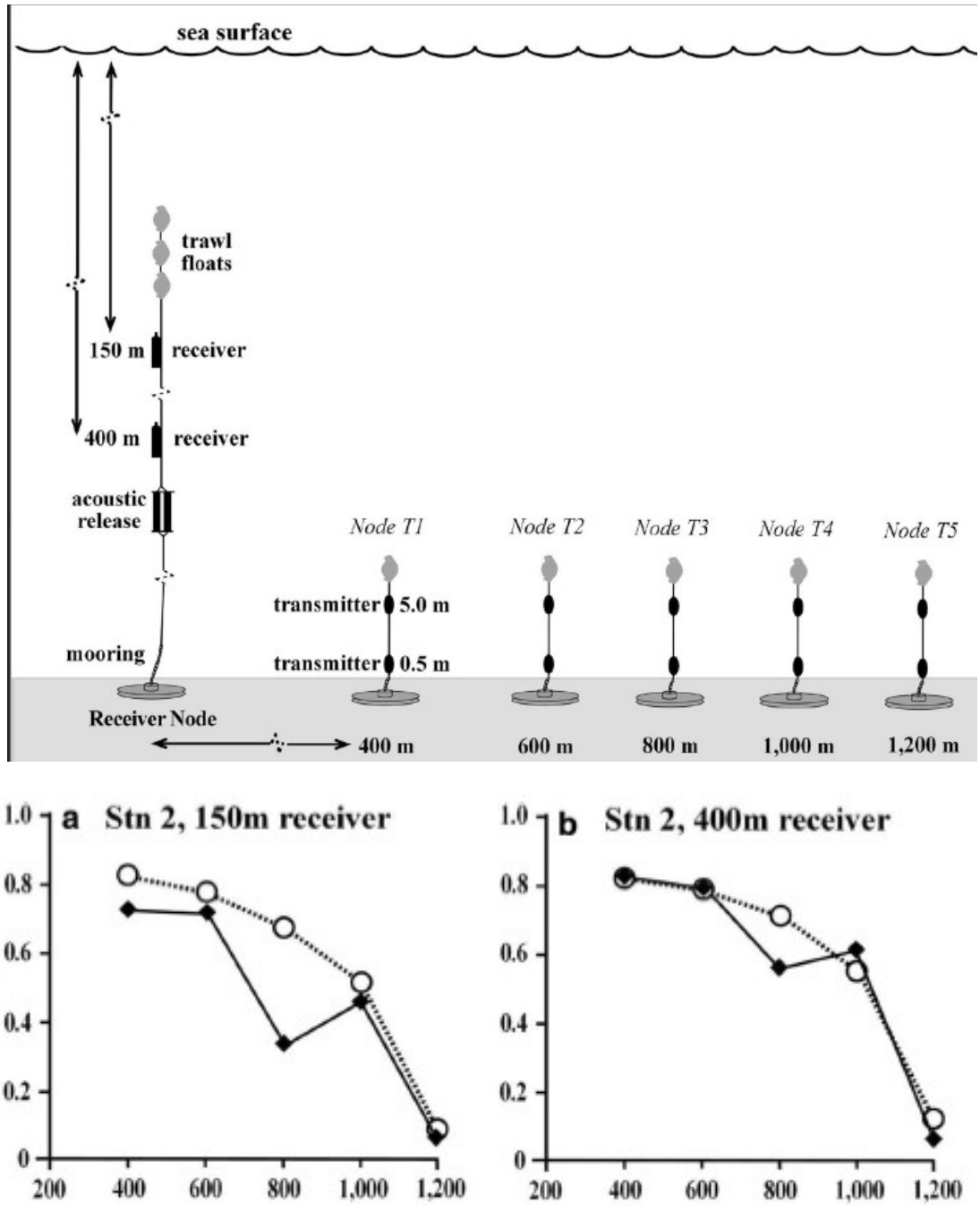

Figure 6: Example of a range testing setup (Top) using the recommended procedure of a statistical analysis of ping detections over time and results (Bottom) displaying probability of detection vs range for station 2 [9].

A literature review of notable fish tag tracking studies reveals varying estimates of detection range for different ocean environments. Wingate et al. [10], focused

on striped bass tagged with V16 tags in the Patuxent River and found the detection range was >500m while providing no upper limit. Secor et al [11] later tested the detection range of this same array and found it to be between 600-1000m.

Loher et al. [9] assessed detection ranges in deep water settings in the North Pacific and found that acoustic transmissions detected by receivers decreased gradually at distances of 400–800 meters and then more steeply at distances beyond 800 meters. The authors state that a linear gate of receivers spaced 1000 meters apart could have episodic periods of poor tag detection, with rates of detectability declining to 60-80%, and below 10% under extreme conditions [9]. It was hypothesized that these extreme conditions were attributed to variations in the acoustic environmental properties which can vary significantly with the changing seasons.

Other studies focused on coastal settings confirmed similar relationships with detectability drop offs over short distances. Kilfoil and Wetherbee [12] found a relatively high detection rate (65% ± 27%; mean ± SD) at 600 meters from receivers in coastal arrays situated in Delaware Bay. However, they also observed a sharp decline in detection efficiency between 600 and 1000 meters, despite a maximum detection range of 1400 meters being recorded. Selby et al. [13] tested detection range for an acoustic receiver array in a shallow water, coral reef habitat (US Virgin Islands), and found that detection probability dropped from

58.2% at 100 meters to 26.0% at 200 meters from a receiver. These studies show that altering array spacing by as little as 100-200 meters can have a significant impact on tag detection, especially if receivers fall within the range of sharp decline in detection efficiency. It is also quite apparent that varying ocean settings (i.e., coastal vs open ocean) impact the effective range of the tags.

Several more recent studies have been dedicated to investigating how detection ranges can be influenced by changing acoustic environments. Goulette and Hawke [14] researched the effect of receiver depth on detection probability in a cold-water estuary habitat (Penobscot Bay, Maine). They found that detection probability improved as much as 18.3% when receivers were placed on the bottom and by 9.2% when receivers were placed at 20 meters versus 10 meters depth. O'Brien and Secor [15] studied the impact of thermal stratification and storms on acoustic telemetry detection in the US Southern Mid-Atlantic Bight and found that an array setup with receivers and sources both below the thermocline can lead to an increase in detectability. The authors also compared the results of several detection range studies (Table 4) showing how coastal receiver array detectability varies with the presence of a thermocline; with implications for the placement in depth and range required to provide proper detection coverage for an area.

Table 4: Reported influence of a thermocline on detectability. Gradient, depth, and respective placement of transmitters and receivers across the thermocline were reported or calculated from reference figures [15].

Reference	System	Thermocline			
		Gradient (°C/m)	Depth (m)	Transmitter–receiver side	Effect on detectability
Present study	Southern Mid-Atlantic Bight, USA	1–2	8–15	Same (below)	+
Oliver et al. [32]	Southern Mid-Atlantic Bight, USA		15–20	Mix	–
Jossart et al. [30]	Caribbean, USVI	0.2	30–40	Within	–
Singh et al. [33]	Kromme Bay, South Africa	1	12–14	Mix	–
Huveneers et al. [29]	New South Wales, Australia	0.44	> 20	Mix	–
Cagua et al. [34]	Red Sea, Saudi Arabia	> 0.04	< 37	Mix	–
Gjelland and Hedger [31]	Lake Skrukkebukta, Norway		10–21	Opposite	–
Klinard et al. [2]	Lake Ontario	> 0.08	11	Mix	–

While varying detectability of receivers is often associated with changing environmental conditions, the effect is not highlighted or is presented without raw acoustic data from experimental field study. Kessel et al. [16] conducted a review of 378 passive acoustic telemetry studies and scored how well they performed range testing on a scale of 0-46 based on a predefined set of criteria. The study revealed that the quality of range testing was inadequate across almost the entirety of literature, with scores ranging from 0 to 39 (11.1 ± 0.4; mean ± 1 SE), and mean scores consistently between 6.7 and 12.9 [16]. This review highlights the need for more effective methods to determine suitable range and probability of detection estimates in the field of passive acoustic telemetry and remote fish tag sensing.

2.3. Environmental Factors Effecting Acoustic Propagation

The acoustic environment is highly variable with regards to location and time, especially within turbid and complex coastal water settings. Changes in the acoustic environment can have drastic implications on the ability of sound to

propagate through the water column. Vemco, the manufacturer of the acoustic telemetry tags used in this study, lists the following as factors influencing detection range; transmission power, signal absorption, line of sight, reflection/refraction, multipath, natural and man-made environmental noise, and the receiving quality of the receiver/hydrophone [7]. Many of these factors are represented mathematically in the passive SONAR equation for a simple, small hydrophone:

$$SNR\ (dB) = SL\ - TL - NL$$

where *SNR* is the signal to noise ratio, *SL* is the source level, *TL* is the transmission Loss, and *NL* is the noise level. Each of the terms are given as a relative intensity in units of decibels (dB) and referenced to a pressure of 1 micro-Pascal (μPa) [3] [16]. As referenced in section 2.1, SNR dictates whether the signal in question is detectable. *SL* is defined as the intensity of a radiated sound at 1 meter from the source and is reported in units of dB re 1 μPa @ 1 m [17].

2.3.1. Spreading and Attenuation

Transmission loss includes the combination of loss due to spreading and attenuation. As sound propagates away from a source it loses intensity. Two simple approximations used to account for this loss are the spherical and cylindrical spreading laws. The loss due to spherical spreading is calculated using the equation below, where sound is assumed to propagate uniformly away from the source in all directions [17] [18].

$$Spherical\ spreading\ loss = 20\log(range\ in\ meters)$$

At some point, sound ceases to propagate uniformly in all directions, as it interferes with the sea surface and seafloor. Cylindrical spreading is used to approximate the spreading loss in a medium with upper and lower boundaries and can be seen in the Equation below [17].

$$Cylindrical\ spreading\ loss = 10\log(range\ in\ meters)$$

These equations for spherical and cylindrical spreading are only approximations of spreading loss however, as they do not consider the effects of refraction within the water column and reflection at the sea surface and seafloor.

Although transmission loss is typically dominated by the laws of spreading, the effects of attenuation are considerable at frequencies as high as 69 kHz. Attenuation is the decrease of sound intensity due to the loss of acoustic energy to heat energy, and its effects are present in both the water column and seafloor [17]. Losses due to attenuation are calculated using an absorption coefficient typically represented in dB per kilometer (dB/km) or wavelength (dB/λ). In the most general case, water column absorption is a function of source frequency and the seawater properties of temperature, salinity, and depth, however some models such as those used in Ainslie-McColm (1998) [20] also consider the effects of acidity (pH). The Francois-Garrison (1982) [21] model for water column absorption (Figure 7) is commonly used to estimate the absorption coefficient at different seawater temperatures and source frequencies. At a frequency of 69 kHz and water temperatures near 20° Celsius, one can infer an estimate of 20 dB/km for water column absorption using the Francois-Garrison model.

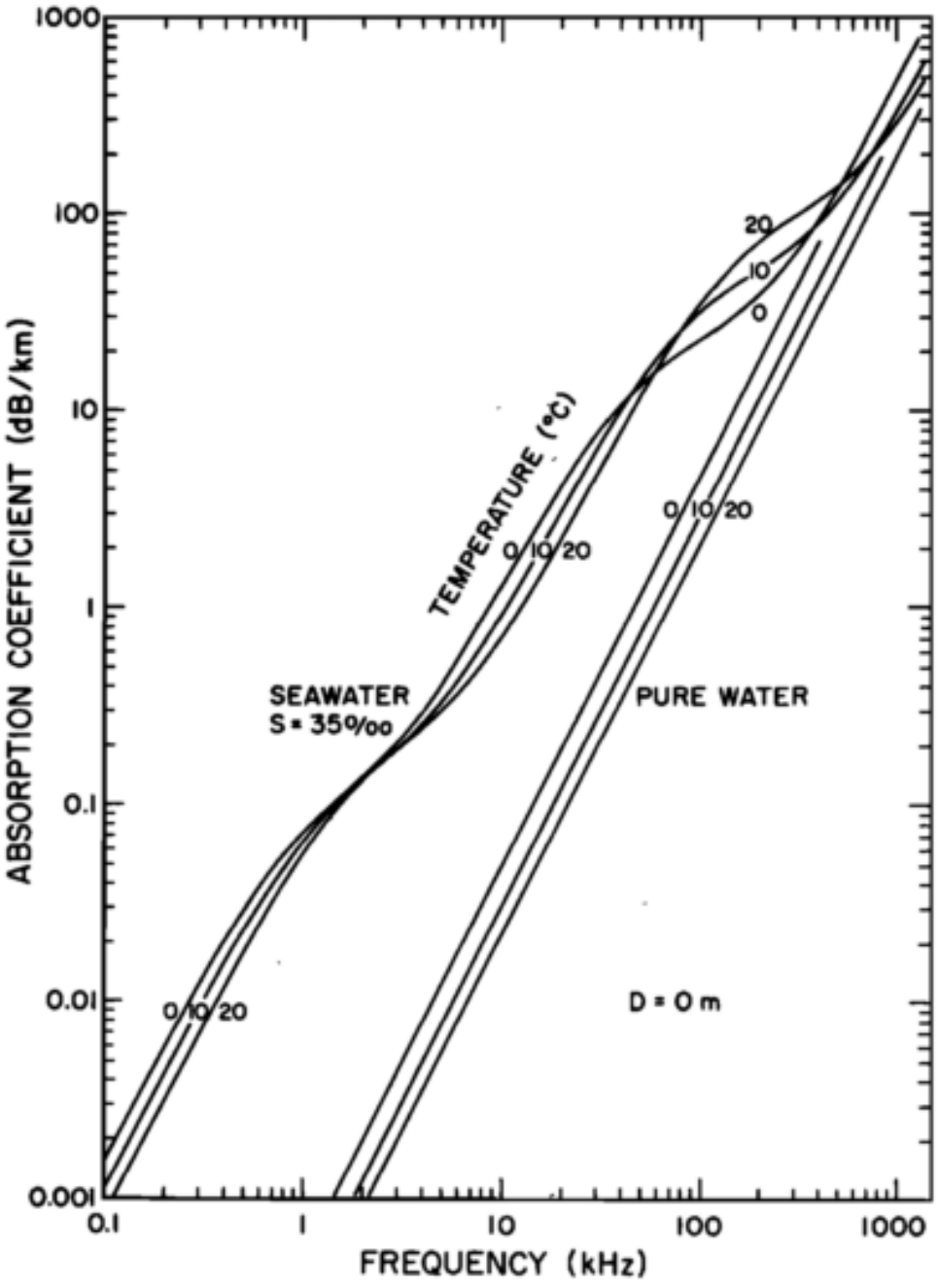

Figure 7: Francois and Garrison empirical model for absorption vs frequency [21].

attenuation experienced in the water column [18] [22]. The acoustic properties and absorption levels of sediment types commonly found on the seafloor (Table 5) include the p-wave attenuation (α_p), denoted in dB/λ, relative density (ρ_b/ρ_w), and p-wave sound speed (c_p) in m/s [23]. Acoustic rays which interact with the seafloor lose energy through process of reflection and transmission. The amount of energy reflected or transmitted into the seafloor for a flat, planar surface is dependent on the dimensionless reflection (V_{ww}) and transmission (V_{wp}) coefficients [23]:

$$V_{ww} = \frac{z_{wp} - 1}{z_{wp} + 1}$$

$$V_{wp} = \frac{2z_{wp}}{z_{wp} + 1}$$

with

$$z_{wp} = \frac{z_p}{z_w}$$

where

$$z_w = \frac{\rho_w c_w}{\sin\theta_w} \text{ and } z_p = \frac{\rho c_p}{\sin\theta_p}$$

are the acoustic impedances of the two mediums, θ_w is the grazing angle of the incident wave vector, and c and ρ are the acoustic properties of sound speed and density for the two mediums (Figure 8). The equations above show how sediment sound speed influences bottom losses. For example, bottom loss is small in sandy sediments for grazing angles less than the critical angle θ_{crit}, where

$$\theta_{crit} = \cos^{-1}(1/v_p)$$

and where v_p is the compressional/water speed ratio in the sediment. As the grazing angle increases to values greater than the critical angle the bottom loss also increases due to a greater fraction of incident energy being transmitted into the seafloor [23]. For a muddy or silty sediment there is no critical angle, and the bottom losses are greatest at the angle of intromission. At the angle of intromission, the transmission of sound across the interface is nearly perfect, as the acoustic impedance of the seafloor matches that of the water column [23].

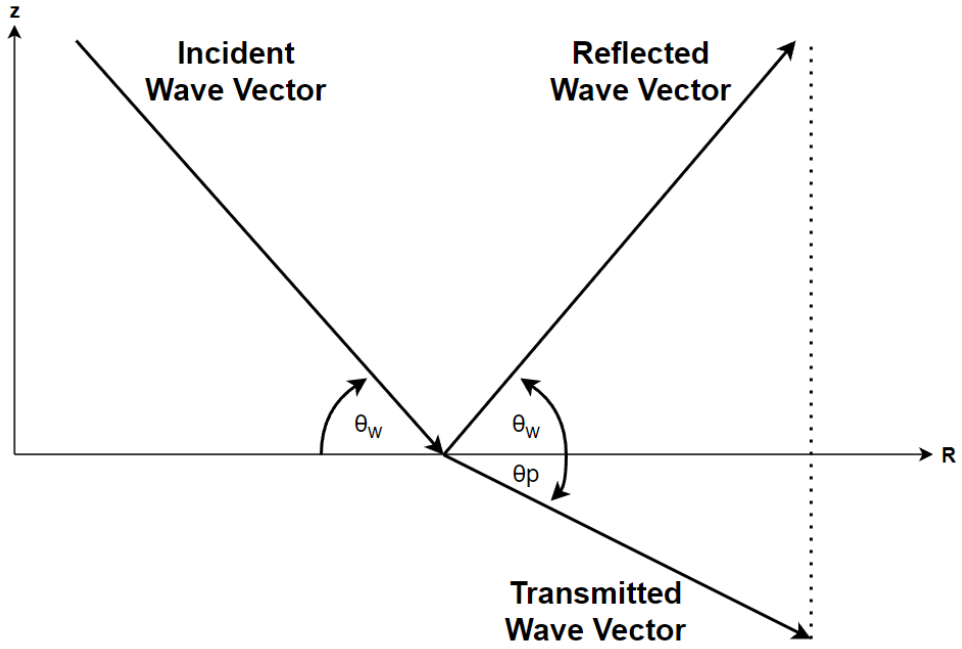

Figure 8: Planar boundary between two dissimilar fluids. Arrows represent wave vectors for an incident plane wave and the resulting reflected and transmitted plane waves [23].

Table 5: Geoacoustic properties of continental shelf and slope environments [23].

Bottom type	p (%)	ρ_b/ρ_w –	c_p/c_w –	c_p (m/s)	c_s (m/s)	α_p (dB/λ_p)	α_s (dB/λ_s)
Clay	70	1.5	1.00	1500	<100	0.2	1.0
Silt	55	1.7	1.05	1575	$c_s^{(1)}$	1.0	1.5
Sand	45	1.9	1.1	1650	$c_s^{(2)}$	0.8	2.5
Gravel	35	2.0	1.2	1800	$c_s^{(3)}$	0.6	1.5
Moraine	25	2.1	1.3	1950	600	0.4	1.0
Chalk	–	2.2	1.6	2400	1000	0.2	0.5
Limestone	–	2.4	2.0	3000	1500	0.1	0.2
Basalt	–	2.7	3.5	5250	2500	0.1	0.2

$c_s^{(1)} = 80\tilde{z}^{0.3}$ $\quad c_w = 1500\,\text{m/s}, \quad \rho_w = 1000\,\text{kg/m}^3$
$c_s^{(2)} = 110\tilde{z}^{0.3}$
$c_s^{(3)} = 180\tilde{z}^{0.3}$

2.3.2. Noise Levels

The detection range of a receiver is highly dependent on noise levels from various sources (e.g., weather, boats, marine life). Noise level (NL) often refers to the ambient noise, or background noise, present at a receiver. Extreme weather events and episodic periods of high wind and waves can raise ambient ocean noise significantly, interfering with signals and reducing detection range [7]. The Wenz curve (1962) [24] (Figure 9) is an effective tool for estimating the average ambient noise levels and sources at different frequency spectra. At 69 kHz, the Wenz curve highlights wind dependent bubble and spray noise as the dominating source of noise. The other sources of noise present at 69 kHz include broadband noise from ships and industrial activity, molecular agitation due to thermal noise, and biologics.

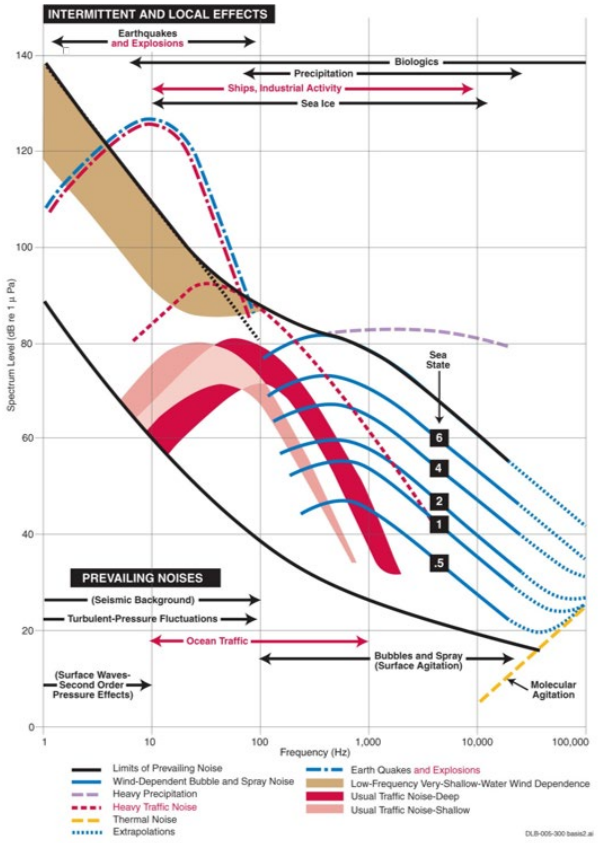

Figure 9: Bradley-Wenz Curves depicting ambient ocean noise levels across different frequencies [25].

The sea state scale used in the Wenz curves is referred to as the Beaufort scale (Table 6) [24]. At 69 kHz, and a sea state between 2-4, average ambient noise levels is estimated at 30-35 dB. However, the Wenz Curve (Figure 9) considers the average noise levels in deep water settings. Wenz [24] states that the shallow-water levels are about 5 dB higher than the corresponding deep-water levels at the same frequency and wind speed, where shallow water is defined as water less than 183 meters in depth. By adding 5 dB, the estimate for average ambient noise levels at 69 kHz becomes 35-40 dB.

Table 6: Beaufort scale showing the relation between wind speed, wave height, and sea state [24].

Sea criteria	Wind speed: Beaufort scale	Wind speed: Range knots (m/sec)	Wind speed: Mean knots (m/sec)	12-h wind: Wave height[a,b] ft (m)	Fully arisen sea: Wave height[a,b] ft (m)	Fully arisen sea: Duration[b,c] h	Fully arisen sea: Fetch[b,c] naut. miles (km)	Sea-state scale
Mirror-like	0	<1 (<0.5)						0
Ripples	1	1–3 (0.5–1.7)	2 (1.1)					½
Small wavelets	2	4–6 (1.8–3.3)	5 (2.5)	<1 (<0.30)	<1 (<0.30)			1
Large wavelets, scattered whitecaps	3	7–10 (3.4–5.4)	8½ (4.4)	1–2 (0.30–0.61)	1–2 (0.30–0.61)	<2.5	<10 (<19)	2
Small waves, frequent whitecaps	4	11–16 (5.5–8.4)	13½ (6.9)	2–5 (0.61–1.5)	2–6 (0.61 1.8)	2.5 6.5	10–40 (19–74)	3
Moderate waves, many whitecaps	5	17–21 (8.5–11.1)	19 (9.8)	5–8 (1.5–2.4)	6–10 (1.8 3.0)	6.5–11	40–100 (74–185)	4
Large waves, whitecaps everywhere, spray	6	22–27 (11.2–14.1)	24½ (12.6)	8–12 (2.4–3.7)	10–17 (3.0–5.2)	11 18	100–200 (185–370)	5
Heaped-up sea, blown spray, streaks	7	28–33 (14.2–17.2)	30½ (15.7)	12–17 (3.7 5.2)	17–26 (5.2–7.9)	18–29	200–400 (370–740)	6
Moderately high, long waves, spindrift	8	34–40 (17.3–20.8)	37 (19.0)	17–24 (5.2–7.3)	26–39 (7.9–11.9)	29–42	400–700 (740–1300)	7

[a] The average height of the highest one-third of the waves (significant wave height).
[b] Estimated from data given in U. S. Navy Hydrographic Office (Washington, D. C.) publications HO 604 (1951) and HO 603 (1955).
[c] The minimum fetch and duration of the wind needed to generate a fully arisen sea.

Total NL is then calculated by adding the bandwidth *BW*, or frequency span of a signal, to the ambient noise levels, as shown in the equation below.

$$NLtotal = NL + 10\log BW$$

NL is calculated at the receiver using either the median or Root Mean Square (RMS) of signal levels. Median noise, as defined by the National Physical Laboratory's guide for underwater acoustic measurement [26], is equivalent to the 50th percentile of the signal levels. The value depends on snapshot time, and it is influenced minimally by high amplitude transient events. RMS noise is defined as the average sound pressure in pascals. It is invariant of snapshot time, however it is sensitive to very high amplitude transient events, such as a

ship passing by. For that reason, the RMS noise can be biased to levels significantly higher than the median (Figure 10), which is considered more representative of background noise levels than RMS [26].

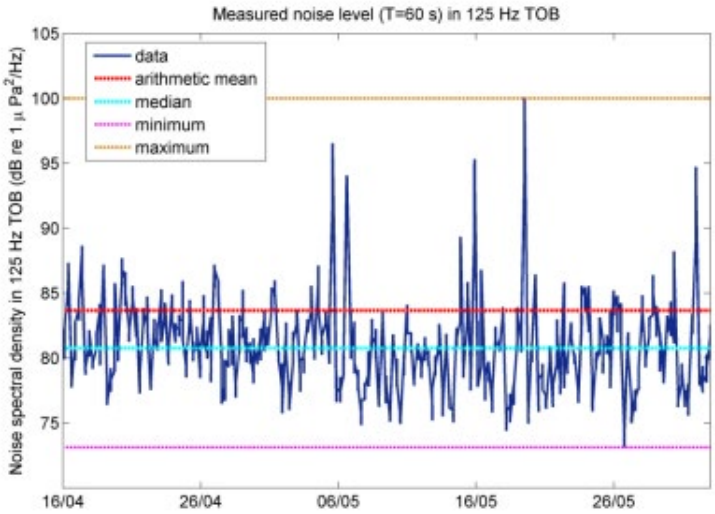

Figure 10: Bias of RMS noise levels as compared to median noise levels due to high amplitude transient events [26]. The median noise level is shown in cyan, and the arithmetic mean, or RMS level is shown in red.

2.3.3. Wave Bending and Refraction

In shallow water coastal regions, such as Narragansett Bay, temperature and salinity profiles that determine sound speed vary significantly with location and time [22]. In the spring and summer months, solar heating warms the ocean surface and creates temperature gradients at depth. Salinity gradients occur in areas where there are freshwater sources, or during times of increased rainfall. Sound waves refract or bend as they move through the sound speed gradients in these regions. The effects of refraction can impact range for certain signal paths, and in some cases, produce shadow zones [8]. Snell's law, shown in the equation below, dictates the refracting nature of sound waves within the ocean,

where θ_1 is the incident angle, θ_2 is the angle of refraction, c_1 is the sound speed of the original medium, and c_2 is the sound speed in the new medium [3].

$$\frac{\sin\theta_1}{\sin\theta_2} = \frac{c_1}{c_2}$$

Snell's Law shows how a sound wave traveling through the ocean refracts and changes its angle of propagation whenever it encounters a change in speed. When sound speed is constant, rays do not refract and propagate in straight lines. This is often the case in winter months when waters become well mixed by wind and waves, resulting in sound speed becoming largely independent of depth [21]. Acoustic energy is evenly dispersed throughout the water column as rays travel in straight lines and reflect off the surface and seabed (Figure 11). Some acoustic energy may be lost at the surface due to scattering in rough weather conditions, however the surface is typically considered a perfect reflector [3]. Rays also reflect off the rough seafloor and lose energy through scattering. If the angle of incidence is greater than the critical angle, typically 15°, rays will enter the seabed and be attenuated. Less than 15° and the seafloor is also considered a perfect reflector [22].

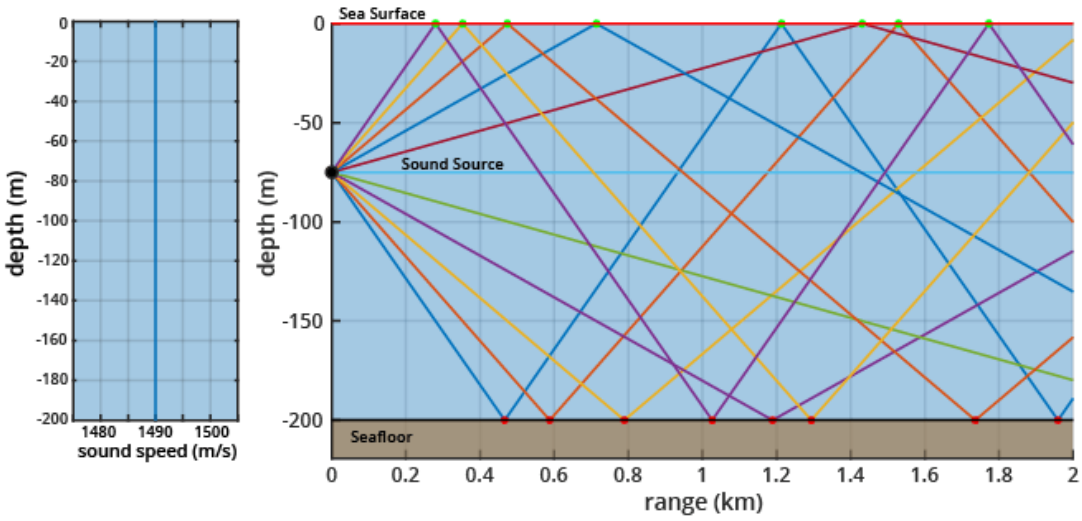

Figure 11: Constant sound speed profile (left) and straight paths followed by sound rays as they propagate away from a source in shallow water. Credit DOSITS [21].

During the spring and summer months, when temperature and salinity gradients are at their highest, the acoustic environment is classified as downward refracting [3] [4]. This is due to the nature of Snell's law and the fact that sound rays bend toward regions with slower sound speeds. Rays propagate away from the source and bend downwards towards the seabed as they traverse through the depths of the thermocline before they can propagate to the surface (Figure 12). A receiver placed at or above the thermocline wouldn't hear the same level of signal as the one placed below. Additionally, rays trapped below the thermocline interact with the seafloor repeatedly, becoming rapidly weaker due to the increased attenuation [22].

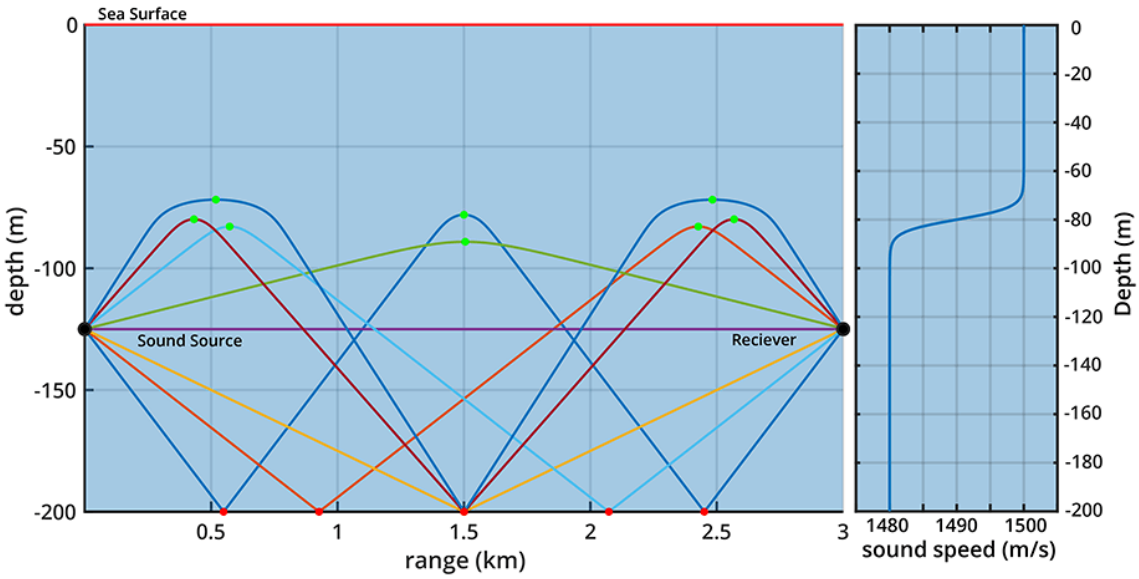

Figure 12: Downward refracting acoustic rays (left) as a result of a sound speed profile gradient (right) from a spring or summer thermocline with a source and receiver located at depths directly below the thermocline Credit DOSITS [21].

2.4. Bellhop and High Frequency Acoustic Modeling

Bellhop is an open-source acoustic propagation program that uses beam tracing for predicting acoustic pressure fields in ocean environments. The program uses geometric and physics-based spreading laws for predicting acoustic pressure fields in ocean environments and can produce a variety of useful outputs including transmission loss, eigenrays, arrivals, and received time-series [27]. The model allows for range-dependence in the top and bottom boundaries (altimetry and bathymetry), as well as in the sound speed profile [27]. Other model inputs include source frequency and depth, receiver depth, seafloor characteristics, altimetry, and top/bottom reflection coefficients. Bellhop is also computationally efficient, especially since ray tracing is independent of source frequency [27]. This makes it an ideal program for modeling high frequency

sound, unlike normal mode models such as Kraken which struggle to converge on solutions at high frequencies due to the generation of Scholte or Stoneley waves [28]. Bellhop is also a widely accepted and frequently utilized tool used to study the propagation of high frequency acoustic propagation of underwater acoustic modems in shallow water environments [29] [30] [31].

2.5. Logistic Regression Analysis and GLM

A logistic regression, or logit model, is a type of generalized linear model (GLM) used to model binary data (0/1, yes/no, detection/no-detection) as the probability of an event occurring or not with one or multiple predictor variables [32]. The logistic function, shown below, produces an s-shaped curve with a probability between 0 and 1, with β_0 and β_1 being the regression coefficients, and *X* the given predictor variable [32]. The simplest predictor variable when considering the relationship between detections and non-detections of acoustic fish tags would be range.

$$p(X) = \frac{e^{\beta_0+\beta_1 X}}{1 + e^{\beta_0+\beta_1 X}}$$

Logistic Regression analysis and GLM's have been used in several studies to estimate the relationship between detection probability and range for Vemco fish tag receivers. The logistic regression is intuitively comparable to the logistic acoustic power loss due to spreading over range and is effective at determining D_{50}, an estimate for range at which probability of detection is 50% [15]. A Vemco sponsored study on receiver performance suggests that 50% probability of detection is the limit in which tags can be reliably detected [33]. In a study

investigating the influence of environmental parameters on the performance and detection range of acoustic receivers, Huveneers et al. (2015) estimated D_{50} by fitting a logistic relationship between detection probability and range, where detection probability was determined by dividing the number of detections recorded by the number of detections expected [34]. Results from Melnychuk & Walters (2010) also validated the use of logistic regression and GLM's as a means for establishing a relationship between range and detection probability [35].

List of References

[1] Vemco. Microsoft PowerPoint - Sydney2007 [Compatibility Mode] (imos.org.au)

[2] Vemco. How do PPM coded tags work? (vemco.com)

[3] Urick, R. J. (1983). Principles of Underwater Sound, Third Edition (3rd edition, Reprint 2013). New York: McGraw-Hill, Inc.

[4] Ziomek, L. J. (1995). Fundamentals of acoustic field theory and space-time signal processing. Boca Raton: CRC Press.

[5] DOSITS. Detection Threshold for Sonar – Discovery of Sound in the Sea (dosits.org)

[6] Vemco. v16-coded-1.pdf (oceans-research.com)

[7] Vemco. How much detection range can I expect from my tags and receivers? (innovasea.com)

[8] Douglas G. Pincock. (2009). Detection Performance of Lines of VR2W/VR3 Receivers. AMIRIX Systems Inc.

[9] Loher, T., Webster, R.A. & Carlile, D. A test of the detection range of acoustic transmitters and receivers deployed in deep waters of Southeast Alaska, USA. Anim Biotelemetry 5, 27 (2017). https://doi.org/10.1186/s40317-017-0142-y

[10] Wingate, R.L., Secor, D.H. and Kraus, R.T. (2011), Seasonal Patterns of Movement and Residency by Striped Bass within a Subestuary of the Chesapeake Bay. Transactions of the American Fisheries Society, 140: 1441-1450. https://doi.org/10.1080/00028487.2011.630279

[11] Secor DH, O'Brien MHP, Gahagan BI, Watterson JC, Fox DA (2020) Differential migration in Chesapeake Bay striped bass. PLoS ONE 15(5):e0233103. https://doi.org/10.1371/journal.pone.0233103

[12] James P. Kilfoil, Bradley M. Wetherbee, John K. Carlson & Dewayne A. Fox (2017) Targeted Catch-and-Release of Prohibited Sharks: Sand Tigers in Coastal Delaware Waters, Fisheries, 42:5, 281-287, DOI: 10.1080/03632415.2017.1306974

[13] Selby, T.H., Hart, K.M., Fujisaki, I., Smith, B.J., Pollock, C.J., Hillis-Starr, Z., Lundgren, I. and Oli, M.K. (2016), Can you hear me now? Range-

testing a submerged passive acoustic receiver array in a Caribbean coral reef habitat. Ecol Evol, 6: 4823-4835. https://doi.org/10.1002/ece3.2228

[14] Goulette, G.S. and Hawkes, J.P. (2017), Altering Vertical Placement of Hydroacoustic Receivers for Improved Efficiency in Coldwater Estuary Zones. North American Journal of Fisheries Management, 37: 981-988. https://doi.org/10.1080/02755947.2017.1336133

[15] O'Brien, M.H.P., Secor, D.H. Influence of thermal stratification and storms on acoustic telemetry detection efficiency: a year-long test in the US Southern Mid-Atlantic Bight. Anim Biotelemetry 9, 8 (2021). https://doi.org/10.1186/s40317-021-00233-3

[16] Kessel, S.T., Cooke, S.J., Heupel, M.R. et al. A review of detection range testing in aquatic passive acoustic telemetry studies. Rev Fish Biol Fisheries 24, 199–218 (2014). https://doi.org/10.1007/s11160-013-9328-4

[17] F. E. White , "Fundamentals of Acoustics by Lawrence E. Kinsler, Austin R. Frey, Alan B. Coppens, and James V. Sanders", The Journal of the Acoustical Society of America 72, 1090-1090 (1982) https://doi.org/10.1121/1.388211

[18] Discovery of Sound in the Sea (DOSITS). Sonar Equation Example: Passive Sonar – Discovery of Sound in the Sea (dosits.org)

[19] Discovery of Sound in the Sea (DOSITS). source level – Discovery of Sound in the Sea (dosits.org)

[20] Ainslie M. A., McColm J. G., "A simplified formula for viscous and chemical absorption in sea water", Journal of the Acoustical Society of America, 103(3), 1671-1672, 1998.

[21] Francois R. E., Garrison G. R., "Sound absorption based on ocean measurements: Part II:Boric acid contribution and equation for total absorption", Journal of the Acoustical Society of America, **72**(6), 1879-1890, 1982.

[22] Discovery of Sound in the Sea (DOSITS). How does sound travel in shallow water? – Discovery of Sound in the Sea (dosits.org)

[23] Jackson, D., & Richardson, M. (2007). High-frequency seafloor acoustics. Springer Science & Business Media.

[24] G. M. Wenz, "Acoustic Ambient Noise in the Ocean: Spectra and Sources," Journal of the Acoustical Society of America, Vol. 34, No. 12, 1962, pp. 1936-1956. doi:10.1121/1.1909155

[25] National Research Council (U.S.) (Ed.). (2003). Ocean noise and marine mammals. Washington, D.C: National Academies Press.

[26] Robinson, Stephen & Lepper, Paul & Hazelwood, Richard. (2014). Good Practice Guide No. 133 Underwater Noise Measurement. National Physical Laboratory.

[27] Porter, M. (2019). The BELLHOP Manual and User's Guide.

[28] Porter, M. (1992). The KRAKEN normal mode program.

[29] Badiey, M. (2015). Fluctuations of Broadband Acoustic Signals in Shallow Water.

[30] Morozs, Nils; Gorma, Wael; Henson, Benjamin; Shen, Lu; Mitchell, Paul; Zakharov, Yuriy (2020): Channel Modeling for Underwater Acoustic Network Simulation. TechRxiv. Preprint. https://doi.org/10.36227/techrxiv.11958852.v1

[31] Pusey, Grant & Duncan, Alec & Smerdon, A.M.. (2009). Analysis of acoustic modem performance for long range horizontal data transmission. 1 - 9. 10.1109/OCEANSE.2009.5278203.

[32] James, Gareth, Daniela Witten, Trevor Hastie, and Robert Tibshirani. 2014. An Introduction to Statistical Learning: With Applications in R. Springer Publishing Company, Incorporated.

[33] Pincock, D. (2009). Detection Performance of Lines of VR2W/VR3 Receivers. AMIRIX Systems Inc. Vemco Division.

[34] Huveneers, C., Simpfendorfer, C.A., Kim, S., Semmens, J.M., Hobday, A.J., Pederson, H., Stieglitz, T., Vallee, R., Webber, D., Heupel, M.R., Peddemors, V. and Harcourt, R.G. (2016), The influence of environmental parameters on the performance and detection range of acoustic receivers. Methods Ecol Evol, 7: 825-835. https://doi.org/10.1111/2041-210X.12520

[35] M.C. Melnychuk., C.J. Walters. Estimating detection probabilities of tagged fish migrating past fixed receiver stations using only local information. Canadian Journal of Fisheries and Aquatic Sciences. 67(4): 641-658. https://doi.org/10.1139/F09-199

CHAPTER 3

METHODOLOGY

The methods are separated into four sections: range testing, data processing, acoustic modeling, and detection range estimation. A series of range tests were conducted throughout Narragansett Bay to measure the receive level of Vemco V16 test tags as a function of range. A stationary hydrophone affixed to a mooring line recorded the acoustic levels of a V16 test tag allowed to drift with the wind and currents on a motor vessel, simulating the movements of a tagged fish. The recorded data (hydrophone receive level, Vemco VR2W detections, GPS tracks) was analyzed using MATLAB (version 2021a) to calculate the receive levels as a function of range. Environmental data (noise level, sound speed, wind speed) collected during testing was analyzed to characterize the effects that varying environmental factors may have on detection range. Acoustic propagation modeling using the Bellhop ray-tracing program was used to predict the levels of transmission loss recorded during range testing. A generalized linear model (GLM) in the form of logistic regression was used to estimate detection probability as a function of range from recorded range testing detections onboard Vemco VR2W receivers. The data from the logistic regression analysis was used to inform the level for a detection threshold in the passive sonar equation where detection probability reached 50%, or D_{50}. Detection ranges were then estimated at the threshold level where the Bellhop modeled output was 5dB above the RMS noise floor. Using this detection threshold, a series of hypothetical modeling scenarios were completed to show

the effects that individual acoustic environmental parameters have on detection range.

3.1. Range Testing

To test the seasonal and environmental effects on high frequency fish tags, field data was collected during the fall of 2020, late spring 2021, and summer of 2021 (Table 7). Environmental data was collected during testing periods to characterize the seasonal variations in the acoustic environment. The primary location for testing was the region between two receivers located within the West Passage near Bonnet Point, however when scheduling permitted data was collected at receiver locations in the East Passage and Sakonnet River (Figure 13).

Table 7: Range Testing Sites and Information.

Date	Test Site	Test Type	V16 depth (m)	Receiver depth (m)	VR2W depth (m)	Sea State	RMS NL (dB)
11/17/20	West Passage	Drift	3/7*	10	8/12	1-2	82
11/19/20	West Passage	Drift	7	10	8/12	2-3	79
05/06/21	West Passage	Drift & Anchor	7	10	7/11	2	80
05/06/21	East Passage	Drift	7	10	8/12	1-2	86.5
06/23/21	Sakonnet River	Drift & Anchor	4	4	2/6	1-2	82
08/04/21	West Passage	Drift & Anchor	7	8	6/10	2-3	85.3

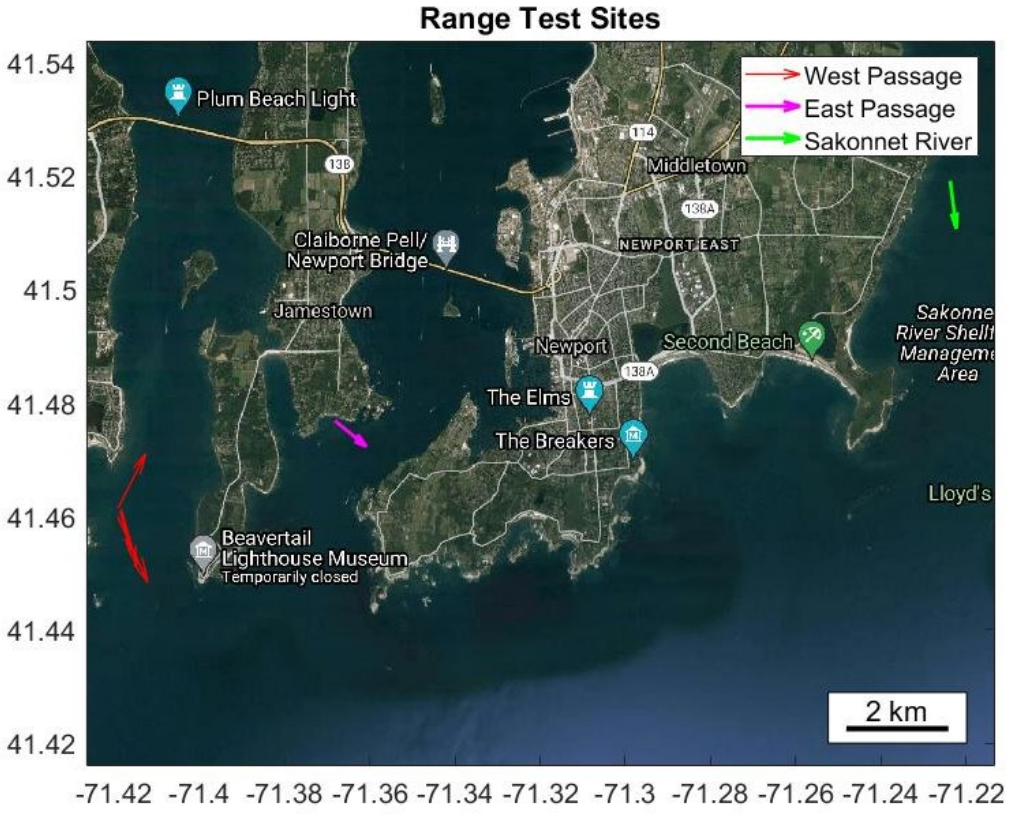

Figure 13: GPS track lines and drift direction from range tests.

3.1.2. Equipment

The resources required for the successful completion of the study were as follows: One Ocean Acoustics Soundtrap hydrophone/datalogger [1], three Vemco VR2W fish tag Receivers [2], two Vemco V16 69 kHz range testing tags [3], one handheld Garmin GPS, one YSI handheld CTD [4] and one Eureka Manta II with handheld Amphibian unit [5], gear to rig testing equipment for deployment including line, shackles, thimbles, anchors, cable ties, floats etc., small vessel time (22ft DEM Eastern motor vessel) in winter/summer, and tank time and laboratory use in the Middleton building acoustics tank. All the

resources listed above were obtained through coordination with the RIDEM Division of Marine Fisheries and URI Ocean Engineering department and federal funding through the U.S Fish and Wildlife Service State Wildlife Grant.

The Vemco V16 range testing tag cycles between Lo/Hi power with a nominal delay of 30 seconds. Tags are activated (on/off) using a magnetic switch attached to the outside of the device. Vemco VR2W receivers listen for and record the serial number of the Vemco tags as well as the time (UTC) to the closest second of detection. VR2W receivers and the Ocean Acoustics Soundtrap were synced to internet time using a field laptop immediately before deployments. The Ocean Acoustics Soundtrap operates as a standalone hydrophone and datalogger capable of recording and logging sound pressure levels onboard the device. At a sampling frequency of 192 kHz the Soundtrap was capable of recording continuously for 90 minutes to a single file. The Soundtrap compresses and saves files in .WAV format and creates new files for continuous lossless recording. Sampling start and stop times (UTC) allowed for accurate time localization of the transmission signals.

3.1.3. Tank Testing

Laboratory tank testing was conducted to measure the ping duration, source level at 1 meter distance, and directivity of the Vemco V16 range testing tags. Tank testing also ensured the test setup and equipment were working correctly before field deployment. The setup of the tank test placed the Ocean Acoustics

Soundtrap hydrophone at 1 meter distance from the Vemco V16 range testing tag (Figure 14).

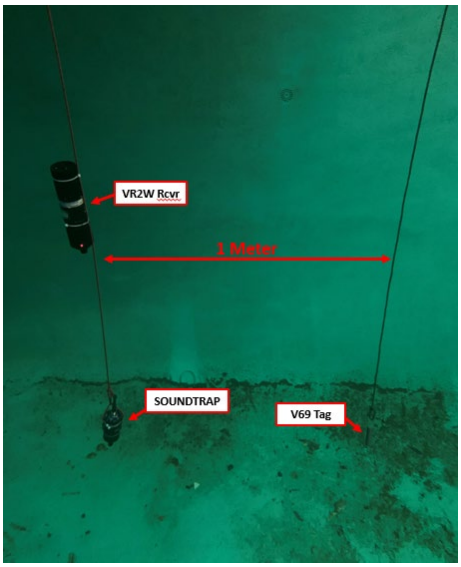

Figure 14: Source Level test setup in the URI OCE Middleton building acoustics tank. Soundtrap is 1m distance from V16 test tag.

The source level test for the V16 test tag was done over a one-hour period. Both high and low power transmission levels were averaged for the entire period of the test. The Hi power SL was calculated to 157.5 dB re 1 µPa @ 1 m (+- 0.6 dB 1 SD), and the low power 152.5 dB re 1 µPa @ 1 m (+- 0.7 dB 1 SD) (Figure 15). Tank testing also revealed that the delay between transmissions of the V16 test tag were a few seconds more than the specified 30 second interval. The delay, although listed at 30 seconds, was not fixed, and varied between 30 to 33 seconds between transmissions.

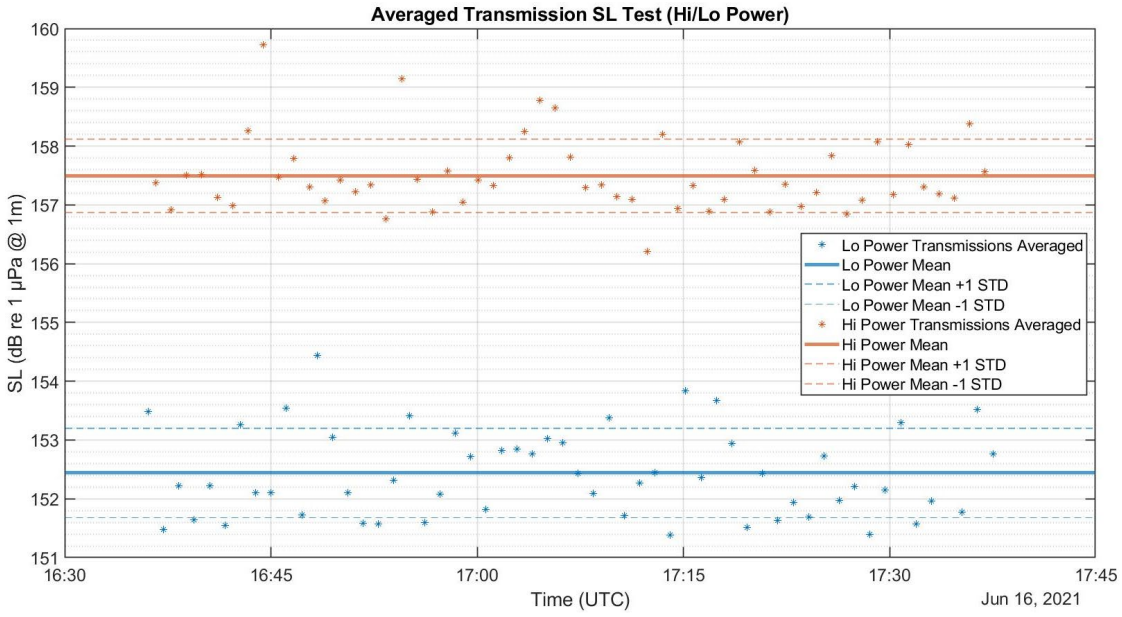

Figure 15: Hi/Lo power source levels recorded during tank testing.

3.1.4. Mooring Design

Two stationary moorings were rigged for range testing use: one for the West and East Passage testing sites, and another for the Sakonnet River testing site. Each mooring used a 25lb mushroom anchor and shackle connected to 9/16-inch Ester-pro brand polypropylene sinking line via a thimble and eye splice. Special consideration was taken to cover all metal-to-metal connection points in electrical tape to mitigate self-noise in the mooring system. The Ocean Acoustics Soundtrap was attached directly to the sinking line using two 50 lb. breaking strength cable ties. Two Vemco VR2W receivers were also attached using cable ties at points equidistant above and below the Soundtrap. Although both the Soundtrap VR2W's are omnidirectional hydrophones, special consideration was taken to orient the receivers with respect to their position in the water column.

The Soundtrap and top VR2W receiver were oriented with the hydrophone downwards, while the bottom VR2W was oriented upwards. The line was held vertically in constant tension by two trawl cans, each with 10 lb.'s of buoyancy. This was done to avoid any self-noise due to pressure fluctuations at the hydrophone from wave action. At the surface, two red floats were affixed to the line via a bowline knot and deployment of the mooring was completed hand over hand (Figure 16). The Sakonnet River mooring was rigged for a shallower depth, with the Soundtrap at a depth of 4 meters and the VR2W receivers at depths of 6 and 2 meters.

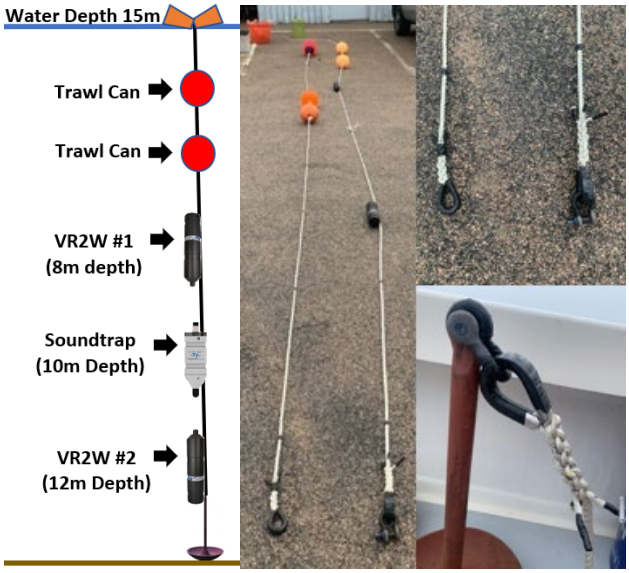

Figure 16: Diagram (Left) of the mooring setup for the West Passage location. Imagery (Right) of the West Passage and Sakonnet river setups.

The drifting tag line consisted of an 8-meter-long sinking line affixed with 25 lbs of dive weights to keep the line vertical and counteract forces due to drag. The tag was affixed to the line with 10lb breaking strength cable ties. During drifts, the

line was lowered to depth and secured to the starboard side of the vessel via a cleat (Figure 17).

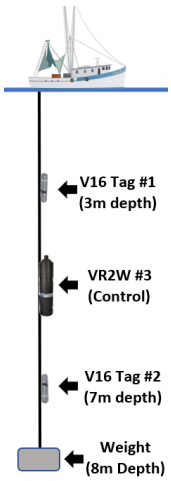

Figure 17: Drifting line diagram with two test tags.

3.1.5. Field Testing

Field testing strategy evolved throughout the course of the project. For the initial testing in November of 2020, the strategy was to measure the acoustic pings of two Vemco V16 range testing tags set at different depths, one shallow and one deep, as a function of distance, from 0-1250 meters. The tag line was accompanied by a Vemco VR2W receiver (control receiver) to decipher when the shallow or deep tags were transmitting at given time intervals. Measurements were recorded using an Ocean Acoustics HF Soundtrap set on a stationary mooring line at a fixed location, approximately 5 meters above the seafloor. The Soundtrap line included two additional VR2W receivers set at depths two meters above and below the Soundtrap to determine whether the test tag pings were recorded at range. On board the vessel, the tag line was lowered so that the two test tags were located at depths of 3 and 7 meters from the sea surface. The

vessel engine was then turned off and the vessel allowed to drift with the movements of the wind and currents.

After analyzing the Vemco VR2W receiver data from the first range test, it was determined that pings from the two range testing tags were colliding during periods of the drift. This was due to the nominal delay of the Vemco V16 fish tags, as discussed in the tank testing section of Chapter 3. Despite attempts to start the tag transmissions 15 seconds apart, the transmissions eventually overlapped one another, and the control receiver could not detect either tag. When tag transmissions collide, it is not possible for the receiver to decipher the serial code from the spacing in between the transmission pings. Due to the colliding transmissions, the period of the drift beyond a range of 700m was unreliable, as it would be impossible to decipher which tag (shallow or deep) was transmitting within the data without the control receiver detecting them. It was concluded that using two range testing tags was not a viable strategy, and therefore one range testing tag at 7 meters depth was used thereafter.

The second attempt at range testing with a single test tag proved to be a viable strategy. The drift provided clear acoustic data without any tag collisions from 0-1250 meters. The range testing methodology was then supplemented with several anchoring stops for set time intervals during the drift. This way, probability of detection estimates could be made at ranges along the drift by determining whether a transmission was detected on the two VR2W receivers

present on the Soundtrap line. This strategy was adopted for all further range testing deployments, except for the East Passage location, where anchoring was not possible with the water depth (40+ meters) and steep bathymetric contours. The drift and anchor strategy (Figure 18) was used at the Sakonnet river test site; however, a separate mooring line adjusted for shallower water depths was used (<7m). Tag and receiver depths were also adjusted accordingly.

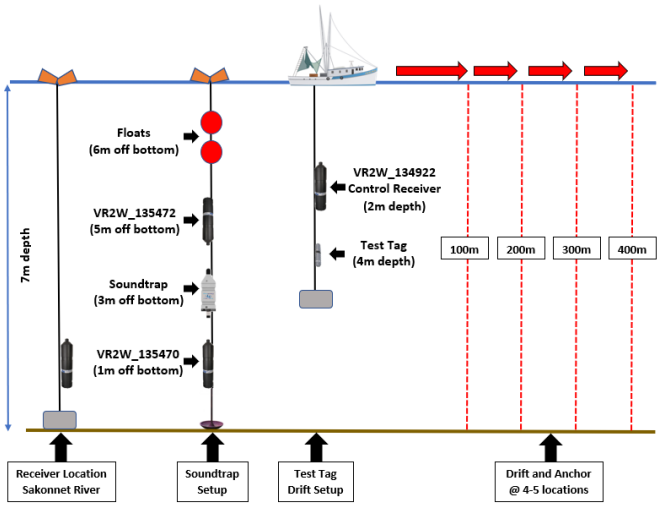

Figure 18: Drift and anchor range testing strategy and schematic for Sakonnet River test site.

During range testing drifts, the vessel was anchored at 5 intervals beginning at around 250 meters away from the fixed Soundtrap line. Successive anchor stops were spaced at approximately 100–200-meter intervals. At each anchor stop, GPS position of the tag line was recorded, and tags remained at depth for 20-25 minutes for a total of 20-25 Hi power test tag transmissions. When conditions in the bay were suitable, the test tag line was lowered into the water and the vessel drifted with the current to 1250 meters range from the Soundtrap line. Testing was completed with the vessel engine turned off to avoid any interference that

vessel noise could have on the transmission range of the tags, except for brief periods to assist in retrieving anchor lines or adjusting drift paths. CTD measurements including salinity, temperature, and depth were recorded for the full water column at the beginning and end of testing, and during anchoring intervals. Time, location, depth, and descriptions of various anthropogenic and self-made (engine noise) noise sources, environmental variables (wind, current, air temperature), mooring deployments, and anchoring intervals were noted. Testing was repeated throughout the year to determine the effects of seasonal and environmental aspects on tag detection.

3.2. Data Processing

Analyses were performed using MATLAB version 2020b. GPS track lines, receiver transmissions as recorded by the Vemco VR2W receivers, and raw acoustic data in *.wav* format from the Ocean Acoustics Soundtrap hydrophone were processed for acoustic modeling. GPS tracks were used to associate each recorded ping with a distance from the hydrophone. Recorded VR2W receiver pings in excel format provided a baseline to show when the tags were transmitting and how far away along the track line the receivers were able to register pings. With the raw acoustic data, the primary interest was to plot the change in receive level of the test tag transmissions as a function of distance along the track line. Only the Hi power test tag transmissions were analyzed during range testing to simplify the data processing. The sampling frequency of the Ocean Acoustics Soundtrap was set to 192 kHz to capture >2x the Nyquist

frequency (69kHz). The MATLAB scripts used to perform this processing can be found in the Appendix.

3.2.1. End-to-End Calibration

The Ocean Acoustics Soundtrap hydrophone and datalogger is provided with a factory provided end-to-end calibration value. The calibration is provided for both high and low gain settings and represents the sound pressure level (SPL) that results in a normalized (±1.0) wav file with a full-scale signal [6]. To convert to units of absolute pressure (μPa), the recorded .wav data is scaled by the end-to-end calibration value.

3.2.2. Demodulation, Decimation, and Filtering

With a sampling frequency as high as 192 kHz, it was necessary to demodulate and decimate the acoustic data to isolate the 69 kHz V16 test tag pings and provide sample sets small enough to be analyzed. A quadrature amplitude demodulation (QAM) was performed using the MATLAB *demod* function. The process of demodulating essentially centered the carrier frequency of 69 kHz around 0 Hz. The MATLAB *decimate* function was then used to resample the sequence in vector X at 1/R times the original sample rate. The resulting resampled vector Y is then R times shorter. By default, *decimate* filters the data with an 8th order Chebyshev Type I lowpass filter with cutoff frequency *0.8*(Fs/2)/R*, before resampling. For better results when R is large (i.e., R > 13), it was recommended to break R up into its factors and calling *decimate* several

times. The *decimate* function was called two times with R = 12 and R = 2. The signal was decimated by a total factor of 24, bringing the bandwidth from 192 kHz to 8 kHz. An additional low pass Butterworth filter with cutoff frequency of 2 kHz was then utilized to remove additional unwanted noise from the signal. The 8 transmission peaks from the Vemco V16 test tag are clearly visible after demodulation, decimation, and filtering (Figure 19). The MATLAB script used to perform this processing is seen in Appendix Listing 1.

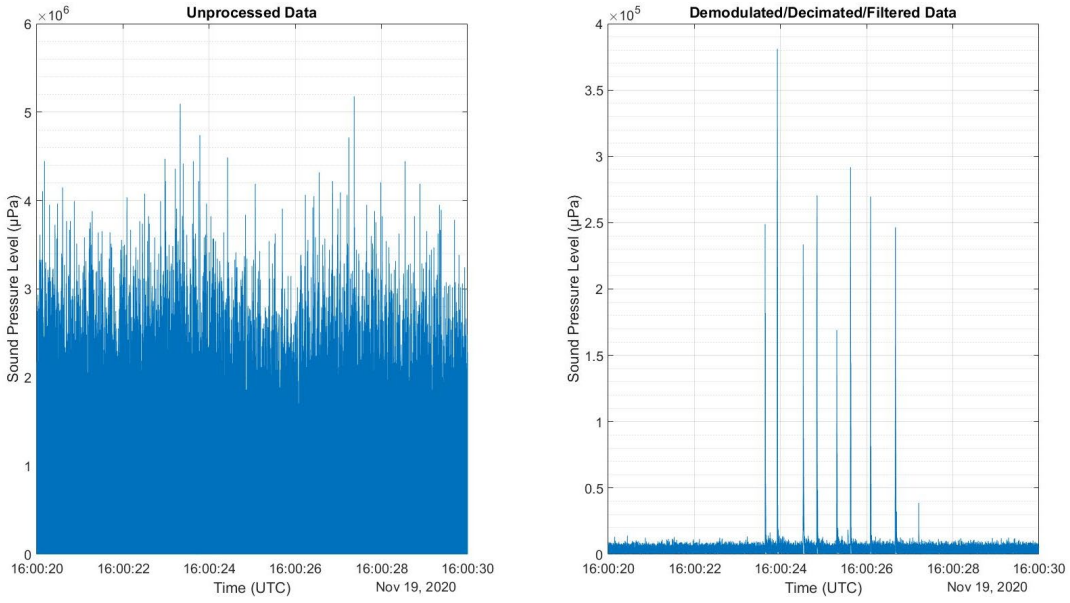

Figure 19: Raw unprocessed acoustic data and demodulated, decimated, and filtered data from range test on 11/19/20 showing a single Hi power V16 tag transmission.

3.2.3. Transmission Peak Averaging

The 8 pings in each Vemco V16 tag transmission were averaged in units of micro-Pascals to quantify the SPL of each transmission. With 100's of transmissions per drift, this process was automated for expedited, consistent

processing. The MATLAB script used to perform this processing is seen in Appendix Listing 2. The MATLAB *findpeaks* function was used to locate the 8 peaks within a range of +- 2.5 seconds of each Vemco VR2W control receiver detection. The mean and standard deviation of the 8 peaks were calculated and recorded for every transmission during a drift. The mean of the transmission peaks was computed in units of absolute pressure (uPa). SPL (dB) re 1 uPa was then calculated using the equation below.

$$SPL(dB) = 20\log\left(\frac{Sound\ Pressure\ (\mu Pa)}{1\ uPa}\right)$$

3.2.4. Noise

RMS and median noise levels were calculated for the entire period of range testing drifts to provide a baseline level for SNR during signal analysis. The entire period of range testing occurred during the time between the first recorded Vemco V16 tag transmission to the last transmission recorded. The average noise levels were computed while in units of absolute pressure (μPa) and then converted to units of decibels (dB) using the equation shown in section 3.2.3. This level was plotted using the MATLAB function *yline* as a constant level across SPL vs Range Figures. Median noise levels were compared to estimated values taken from wind data and the Wenz curves. RMS values were used to make detection probability estimates.

3.2.5. SSP and Absorption

SSP levels were calculated from CTD data using Medwin's equation for sound speed and a series of scripts to read, parse, and plot CTD data. The Medwin [7] equation computes sound speed using conductivity *S* (ppt), temperature *T* (Celsius), and depth *z* (meters). The MATLAB scripts for these functions can be seen in Appendix listings 3-6.

$$c(\frac{m}{s}) = 1449.2 + 4.6 * T - (5.5 * 10^{-2}) * T^2 + (2.9 * 10^{-4}) * T^3$$
$$+ (1.34 - 10^{-2} * T) * (S - 35) + (1.6 * 10^{-2}) * z$$

Depth dependent absorption levels were computed using an empirical formula from Ainslie and McColm [8], which use values of frequency, salinity, temperature, depth, and pH to determine a value for absorption in dB/km. Levels for pH weren't recorded when the YSI CTD was not available (November testing only. Spare CTD provided by DEM was used). For these cases a constant pH of 8.0 was assumed for the entire depth of the water column. Absorption levels were converted from dB/km to dB/λ for later use in modeling.

3.2.6. Wind Data

Wind data was collected from the nearest NOAA NDBC weather station to range testing sites, NOAA station NWPR1 (Figure 20). Data was downloaded and read from historical, quality-controlled CSV files for during times of range testing. Wind speed was recorded in units of m/s by NOAA NDBC as an 8-minute average, and wind gusts were recorded as 6 sec peaks during those 8-minute periods. Wind direction, reported 0-360° clockwise from North, was also provided. Once

downloaded, wind speed was converted to units of knots to associate levels to the Beaufort scale (Table 6).

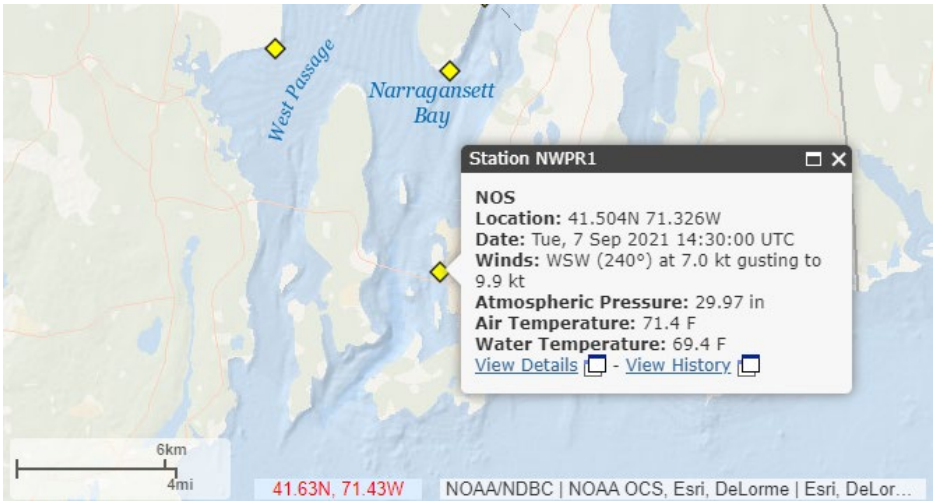

Figure 20: NOAA NDBC station NWPR1 used for wind data collection.

3.3. Acoustic Modeling

Data collected during range testing was evaluated against (and included in) the Bellhop acoustic propagation model to quantify the seasonal and environmental effects of the acoustic environment on high frequency tag detection. Modeled output of transmission loss was subtracted from the source level to calculate the SPL as a function of range. Modeled SPL was compared to and validated by the Vemco V16 test tag receive levels measured during each of the 6 range tests. By validating the acoustic modeling approach with the collected field data, hypothetical scenarios could be modeled with varying environmental parameters (SSP, seafloor type, receiver depth) to see how individual changes effect detection ranges.

3.3.1. Bellhop Setup and Execution

The most recent (2021) release of the Ocean Acoustics MATLAB Toolbox [9] was used to run the Bellhop program. Bellhop is run in MATLAB using setup files referred to as environmental files. These files specify the input values of several environmental variables and modeling parameters. Acoustic properties of the seafloor were inferred using Table 5 in Chapter 2 and based off studies done by the USGS [10] and McMaster [11] to classify sediment types in RI waters. Bottom topography was inferred using depths recorded during CTD profiles and with the transducer aboard the DEM's 22ft Eastern powerboat. NOAA bathymetric data was also downloaded and plotted over GPS track lines to identify any extreme contours or variations in bottom topography. Water depth was modeled as range independent to simplify the model for the West Passage, Sakonnet River, and BI locations as the bathymetry contours were relatively constant over a range of 1 km. The East Passage location was the only model with range dependent bathymetry. Common modeling parameters between all environmental files are listed in Table 8. The parameters that vary included time and location specific SSP and absorption levels, location specific bottom characteristics, and range dependent bathymetry, some of which is seen in Table 9. Source depth was modeled to match the design utilized in range testing. To execute Bellhop, the script seen in Appendix Listing 7 was used.

Table 8: Common model parameters for Bellhop environmental files.

Freq. (kHz)	SSP Interp.	Att. Units	Surface Type	Bottom Type	Ray Angles	Run Type	#Beams	Step Size (m)	Range (km)
69	C-Linear	dB/λ	Vacuum	Acoustic half space	+- 30°	Incoherent TL/Gaussian beam (IB)	100	0.2	1.25

Table 9: Model parameters by location.

Model Site	SSP Data Source	SSP/BTY Range Dependence	Water depth (m)	Source depth (m)	Receiver depth (m)	Bottom Type
West Passage	Field	No	15	7	1/10	Sand
East Passage	Field	Yes	15-40	7	1/10	Sand
Sakonnet River	Field	No	7	4	1/4	Silt
Block Island	RISWAP	No	30	15	1/25	Sand

3.4. Detection Range Estimation

A detection threshold level was set at 8 dB above recorded RMS noise levels for 50% probability of detection range, or D_{50}. The decision to set this threshold at a level of 8 dB above RMS noise level was informed by the binary output (detection/no-detection) of recorded Vemco VR2W receiver data fit with a logistic regression curve for each of the 6 range tests. Examining the probability of detection measurements through logistic regression analysis, it was determined that D_{50} detection range was met between ranges of 675 – 900 meters. At these ranges, the predicted output from the Bellhop acoustic propagation model reached levels of 6.9-9.0 dB above RMS noise level for the individual tests. Rearranging terms from the passive sonar equation, the D_{50} detection range was inferred where the detection threshold level was met by the transmission loss (TL) output from Bellhop and the recorded RMS noise level (NL) subtracted from the source level (SL).

$$DT\ (8\ dB) = SL\ (157.5\ dB) - TL - NL$$

The percent error between the Bellhop model and the logistic regression estimates for D_{50} detection range was determined by measuring the difference in range between the two predictions for each of the 6 range tests.

3.4.1. Logistic Regression

The *glmfit(X,y,distr)* MATLAB function was used to model a simple logistic regression fit for probability of detection corresponding to the single predictor variable (*X*) of range for each of the 6 field tests (Appendix Listing 8). The GLM was computed using a binomial distribution of the response variable (*y*) and a built-in '*logit'* (logistic regression) link function of the form

$$f(\mu) = log(\mu/(1 - \mu)).$$

The response variable (y) is the binary response (detection/no-detection) from the VR2W receivers during range testing. The predictor variable (X) is the range in meters of each binary response. The function *glmfit* returns the coefficient estimates (*b*), deviance (*dev*), and several other statistical parameters (*stats*) such as degrees of freedom, dispersion, covariance, and residuals of the GLM. Using the coefficient output (*b*) of *glmfit* and a range vector with linearly spaced intervals (0-1250 meters) a GLM curve fit was computed using the *glmval* MATLAB function. The *glmval* function was also used to determine 95% confidence intervals for the GLM with the *stats* output of the *glmfit* function.

List of References

[1] Ocean Acoustics Inc. Soundtrap ST300 specification sheet. SoundTrap-300-Spec.pdf (oceaninstruments.co.nz).

[2] Vemco. VR2W receiver specification sheet. vr2w-1.pdf (oceans-research.com).

[3] Vemco. V16 tag specification sheet. v16-coded-1.pdf (oceans-research.com)

[4] YSI 6920 V2-2 Multiparameter Water Quality Sonde. SECTION 1 INTRODUCTION (ysi.com)

[5] Eureka Manta II with Amphibian handheld unit. Brochures for Manta and Eureka Waterprobes instrumentation

[6] Ocean Acoustics Inc. Soundtrap ST300 Manual. www.oceaninstruments.co.nz/wp-content/uploads/2015/04/ST-User-Guide.pdf

[7] Herman Medwin , "Speed of sound in water: A simple equation for realistic parameters", The Journal of the Acoustical Society of America 58, 1318-1319 (1975) https://doi.org/10.1121/1.380790

[8] Michael A. Ainslie and James G. McColm , "A simplified formula for viscous and chemical absorption in sea water", The Journal of the Acoustical Society of America 103, 1671-1672 (1998) https://doi.org/10.1121/1.421258

[9] Ocean Acoustics Toolbox OALIB (oalib-acoustics.org)

[10] McMullen, K.Y., Poppe, L.J., Blackwood, D.S., Nardi, M.J., and Andring, M.A., 2015, Sea-floor morphology and sedimentary environments in southern Narragansett Bay, Rhode Island: U.S. Geological Survey Open-File Report 2015–1149, 1 DVD-ROM, http://dx.doi.org/10.3133/ofr20151149.

[11] Robert Luscher McMaster; Sediments of Narragansett Bay system and Rhode Island Sound, Rhode Island. Journal of Sedimentary Research 1960; 30 (2): 249–274. doi: https://doi.org/10.1306/74D70A15-2B21-11D7-8648000102C1865D

CHAPTER 4

FINDINGS

The findings presented show results from the 6 range tests performed in Narragansett Bay throughout 2021-2022. For each individual range test, measured receive level (dB) for tag transmissions are plotted against range and compared to the predicted output from the Bellhop ray tracing program. Probability of detection was estimated using VR2W detection data and a GLM with a binomial distribution and logistic regression link function. The GLM results ($\boldsymbol{D_{50GLM}}$) informed a detection threshold level where modeled detection ranges ($\boldsymbol{D_{50MDL}}$) were inferred at the range where modeled output was 8 dB above the RMS noise level. A series of detection matrices characterize the effects that seasonal and environmental changes have on tag detection by showing $\boldsymbol{D_{50MDL}}$ detection ranges for several hypothetical modeling scenarios.

4.1. Range Testing Overview

A total of 6 range testing drifts were completed for locations in Narragansett Bay; 4 tests in the West Passage, 1 in the East Passage, and 1 in the Sakonnet River. The results for range testing (Table 10) include the detection range determined through a GLM logistic regression analysis ($\boldsymbol{D_{50GLM}}$), the difference in level (dB) between the Bellhop modeled output and the RMS noise floor, detection range determined from the detection threshold (8 dB) and Bellhop acoustic propagation model ($\boldsymbol{D_{50MDL}}$), and the associated error between the two ranges. The testing days in the East Passage and West Passage with the highest noise levels (>85 dB) are those with the least $\boldsymbol{D_{50MDL}}$ detection range (690 meters), while the West

Passage tests in May and November with the lowest recorded noise levels (<80 dB) had the furthest $\boldsymbol{D_{50MDL}}$ detection range.

Table 10: Range testing results.

Date	Test Site	Sea State	RMS NL (dB)	GLM Range D_{50} (m)	Model-NL @ D_{50} (dB)	Model Range D_{50} (m)	Model Error (%)
11/17/20	West Passage	1-2	82	775	7.8	770.0	0.65
11/19/20	West Passage	2-3	79	837	9.0	867.5	3.64
05/06/21	West Passage	2	80	900	6.9	878.8	2.36
05/06/21	East Passage	1-2	86.5	985	-3.1	693.7	29.57*
06/23/21	Sakonnet River	1-2	82	767	7.8	746.0	2.74
08/04/21	West Passage	2-3	85.3	672	8.5	688.7	2.49

*Two test tags used.
*East Passage GLM not well informed.

4.2. West Passage Data and Model

Range testing in the west passage was performed a total of 4 times during November (2x), May, and August. The bathymetry of the West Passage along range testing track lines was assumed to be constant, as the depth varied <2m (Figure 21).

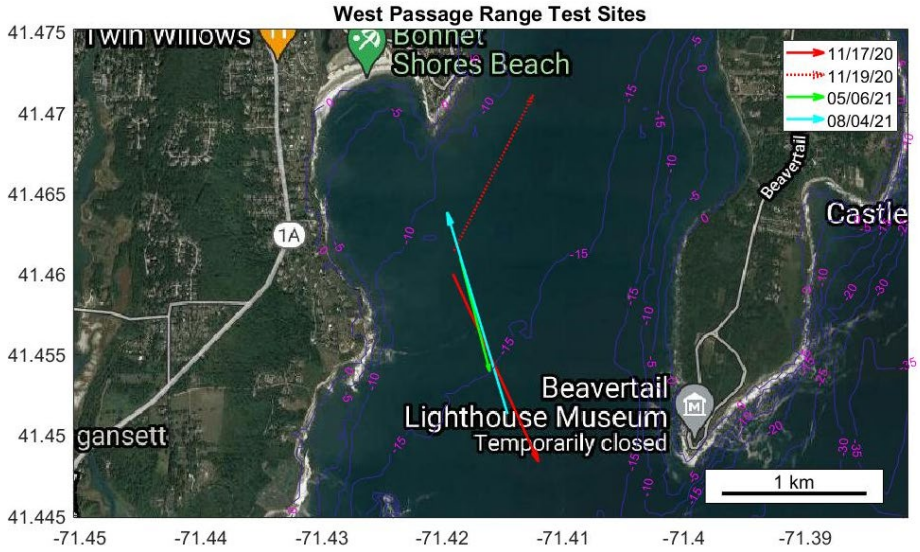

Figure 21: West Passage range test GPS track lines and directions plotted over bathymetry contours (meters) for Narragansett Bay.

4.2.1. November 2020

On 11/17/20 the $\boldsymbol{D_{50GLM}}$ detection range was 775 meters (Figure 22). At this range the model level is approximately 7.8 dB above the RMS noise level. With a detection threshold of 8 dB above RMS NL the $\boldsymbol{D_{50MDL}}$ detection range was 770 meters (0.65% error). A relatively constant sound speed profile (Figure 23) and a modest sea state of 1-2 provided adequate conditions for transmission range. The drift persisted to a range of about 750 meters, and due to technical problems with using 2 range testing tags the drift was abruptly stopped. Minimal tag return data and VR2W detections/non-detections reveal large confidence bounds in the GLM logistic regression.

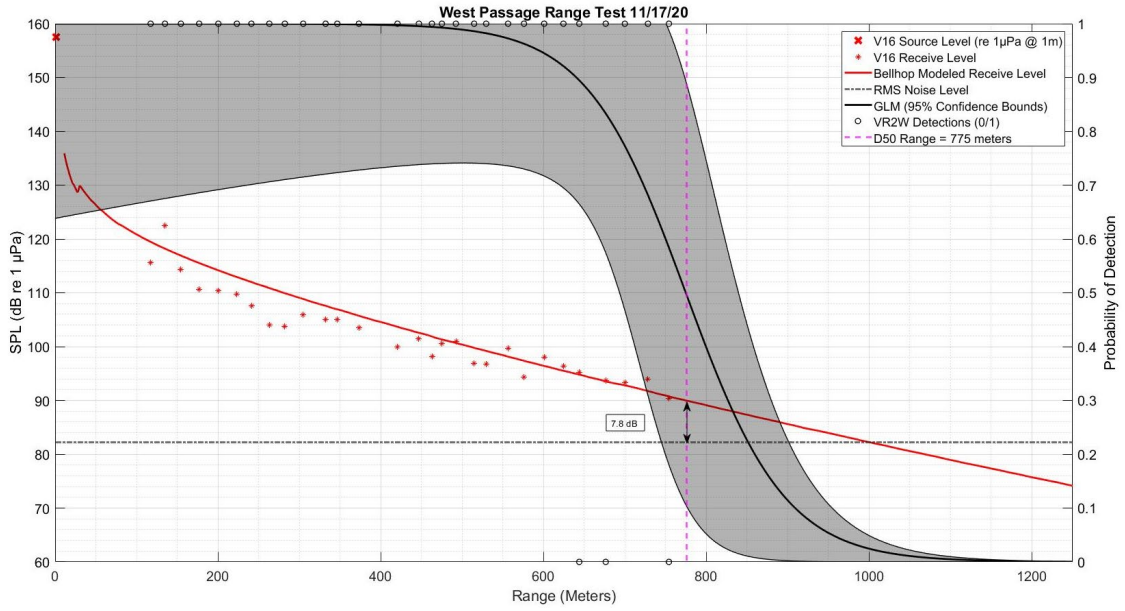

Figure 22: SPL of Vemco V16 test tags as a function of range for West Passage range test (11/17/20). GLM logistic regression for VR2W detections vs. non-detections showing probability of detection with range. Difference between Bellhop model level and RMS noise level is shown at D_{50} range.

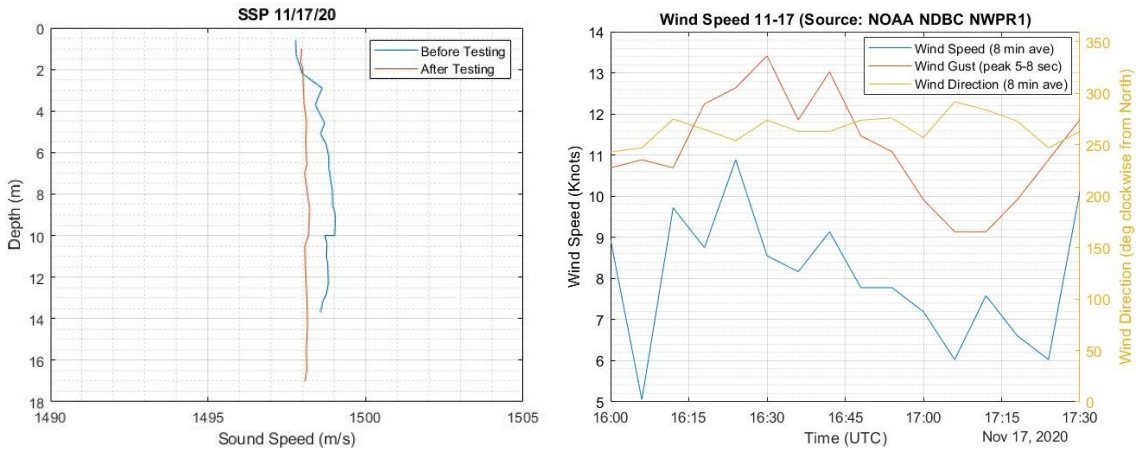

Figure 23: SSP (Left) and wind speed (Right) data for West Passage 11/17/20.

The maximum detection range during the drift on 11/19/20 was 1060 meters, with the VR2W receiver at 8m depth recording the final detection (Figure 24). $\boldsymbol{D_{50GLM}}$ detection range was 837 meters (Figure 24), and at this range the model level was approximately 9.0 dB above the RMS noise level. The $\boldsymbol{D_{50MDL}}$ detection range was calculated as 867.5 meters (3.64% error). With a similar sound speed profile as day 1 of testing (Figure 25), the slight increase in range from 11/17/20 to 11/19/20 can be related to the decrease in RMS noise levels. Although there were increased wind speeds and a greater sea state of 2-3, RMS levels on 11/19/20 were 3 dB lower than on 11/17. The decrease in RMS levels may be associated with increased ship traffic observed during range testing on 11/17/20, as it is possible that RMS noise bias is present due to loud transient events.

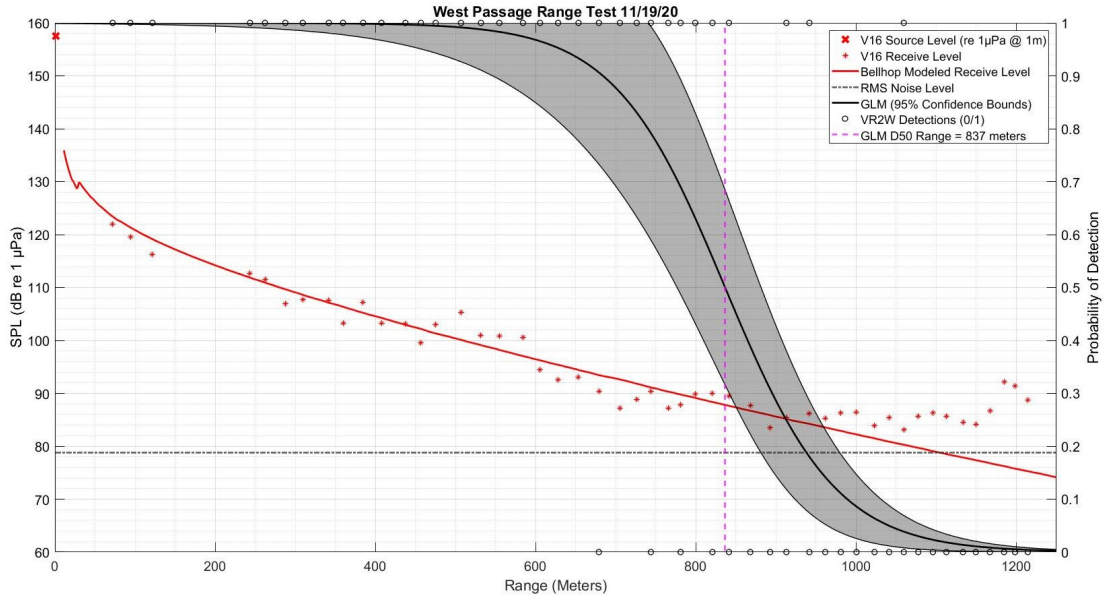

Figure 24: SPL of Vemco V16 test tags as a function of range for West Passage range test (11/19/20). GLM logistic regression for VR2W detections vs. non-detections showing probability of detection with range. Difference between Bellhop model level and RMS noise level is shown at D_{50} range.

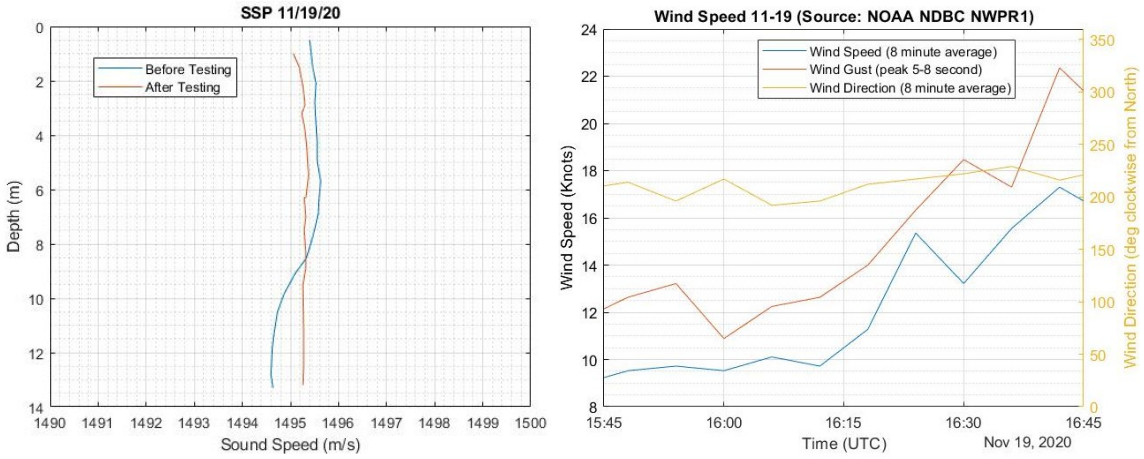

Figure 25: SSP (Left) and wind speed (Right) data for West Passage 11/19/20

4.2.2. May 2021

On 05/06/20 the $\boldsymbol{D_{50GLM}}$ detection range was 900 meters (Figure 26). At this range the model level is approximately 6.9 dB above the RMS noise level. With a detection threshold of 8 dB above RMS NL the $\boldsymbol{D_{50MDL}}$ detection range was 878.8 meters (2.36% error). The maximum detection range during the May West Passage drift is unknown, as testing ceased after the final anchor position, however the $\boldsymbol{D_{50MDL}}$ range is the furthest of all the testing done. This increased range can be attributed to very low RMS noise levels (80 dB) as well as the location of the receiver and source being located below the thermocline (Figure 27). Very little ship traffic and a sea state of 1-2 can be attributed to the low noise levels.

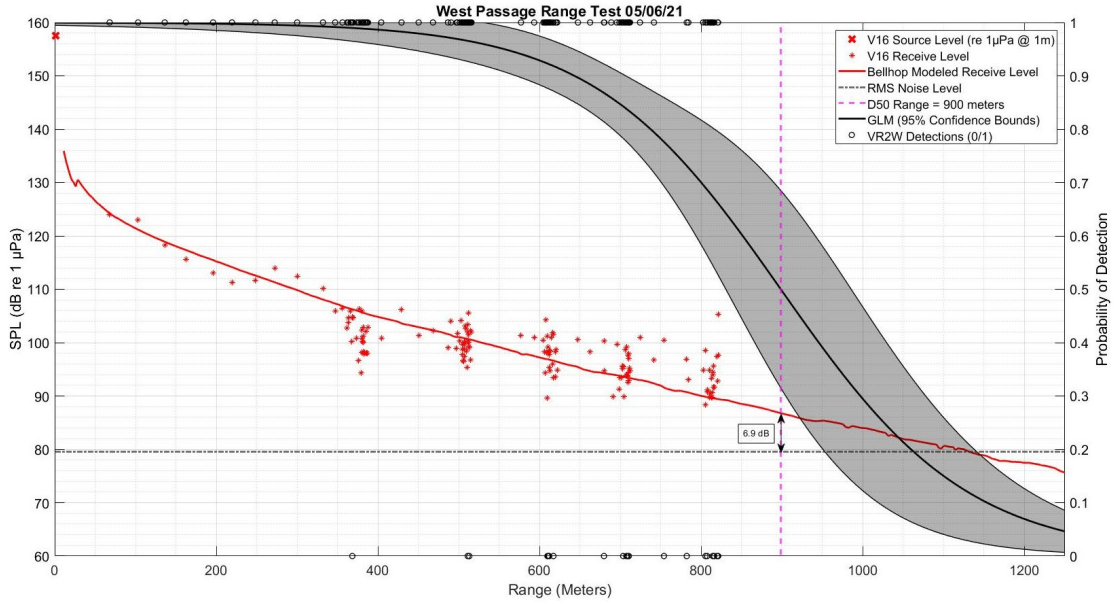

Figure 26: SPL of Vemco V16 test tags as a function of range for West Passage range test (05/06/21). GLM logistic regression for VR2W detections vs. non-detections showing probability of detection with range. Difference between Bellhop model level and RMS noise level is shown at D_{50} range.

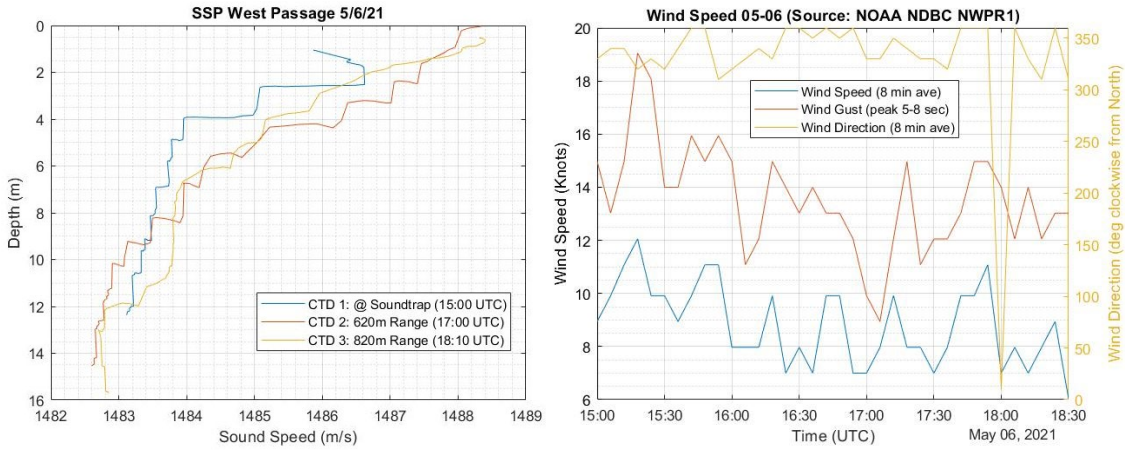

Figure 27: SSP (Left) and wind speed (Right) data for West Passage 05/06/21

4.2.3. August 2021

On 08/04/21 the $\boldsymbol{D_{50GLM}}$ detection range was 672 meters (Figure 28). At this range the model level is approximately 8.5 dB above the RMS noise level. The testing on this day shows a good example of a well-informed GLM logistic regression, as anchoring was done at quality spaced intervals and the drift continued to a range of 1200 meters. The $\boldsymbol{D_{50MDL}}$ detection range was 688.7 meters (2.49% error), making it the lowest of all the range tests. High RMS noise level (85 dB) can be attributed to lots of recorded ship traffic, including multiple occurrences of large vessels (BI Ferry, Fishing/Sailing Vessels) approaching within proximity to the Soundtrap. High sustained winds (10-15 knots) and a sea state of 2-3 would have played a factor in the higher noise level. A significant thermocline (Figure 29) may have also impacted the detection range, as downward refracting rays interact with the seafloor more often and at a higher grazing angle.

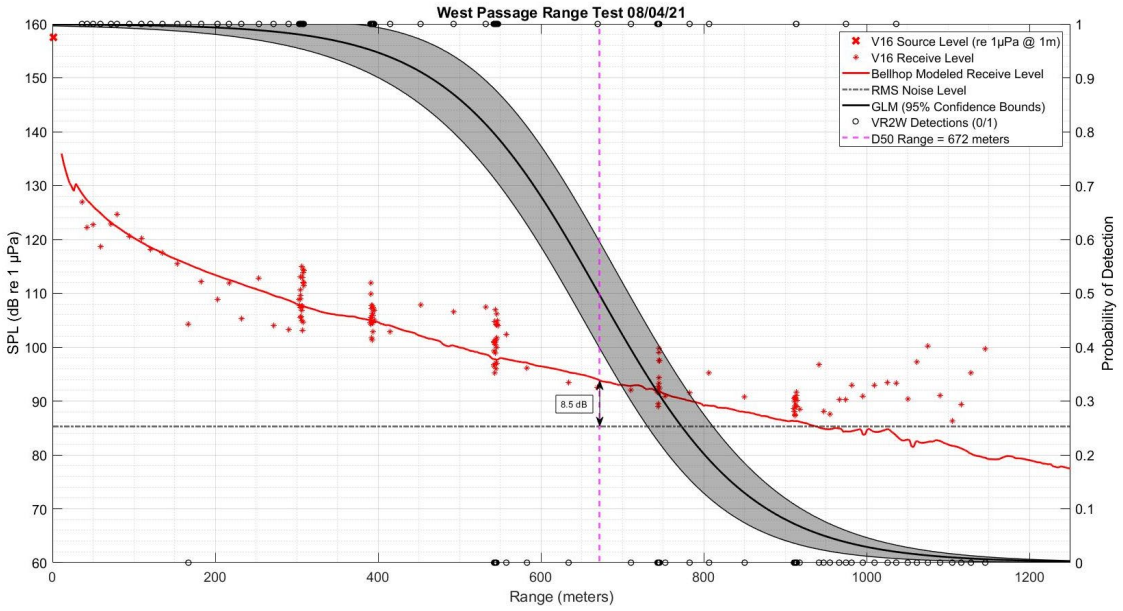

Figure 28: SPL of Vemco V16 test tags as a function of range for West Passage range test (08/04/21). GLM logistic regression for VR2W detections vs. non-detections showing probability of detection with range. Difference between Bellhop model level and RMS noise level is shown at D_{50} range.

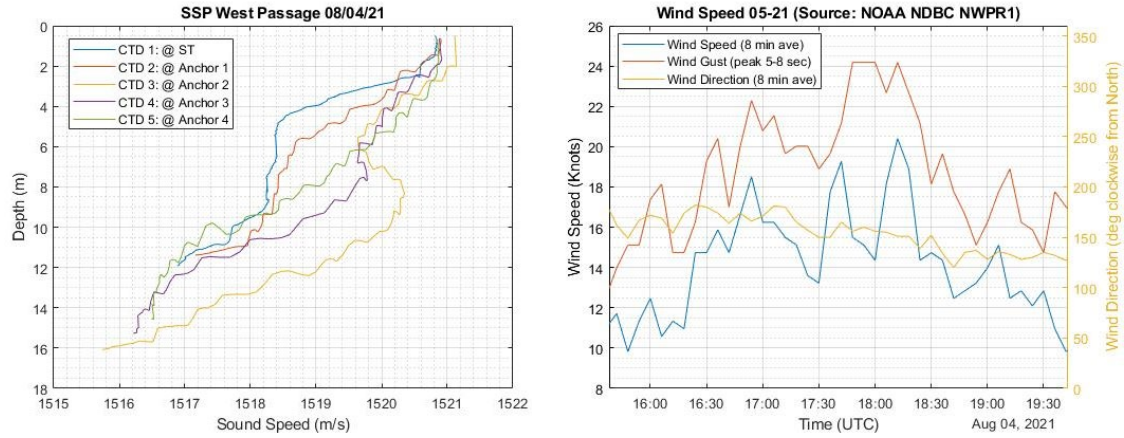

Figure 29: SSP (Left) and wind speed (Right) data for West Passage 08/04/21.

4.3. East Passage Data and Model

The East Passage range test site was the only one of the studies with range dependent bathymetric contours (Figure 30). On 05/06/21 the $\boldsymbol{D_{50GLM}}$ detection range was 985 meters (Figure 30). At this range the model level is approximately

3.1 dB below the RMS noise level. The testing on this day shows an example of a poorly informed GLM logistic regression, as no anchoring was done, and the south easterly drift continued across the shipping channel to a range of 800 meters. The $\boldsymbol{D_{50MDL}}$ detection range was 693.7 meters (2.49% error), making it the second lowest of all the range tests. This test exhibited high NL like the West Passage test site in August. The East Passage test site is a shipping channel with high traffic, and over 10 vessels were recorded passing through the vicinity during testing. Additionally, the Soundtrap was located within 50 meters of a cliff with breaking waves. Both factors can be associated with the increase in RMS noise levels and decreased detection range. The location also had a significant thermocline (Figure 31) and steep bathymetric contours which may have led to more bottom loss due to downward refracting rays.

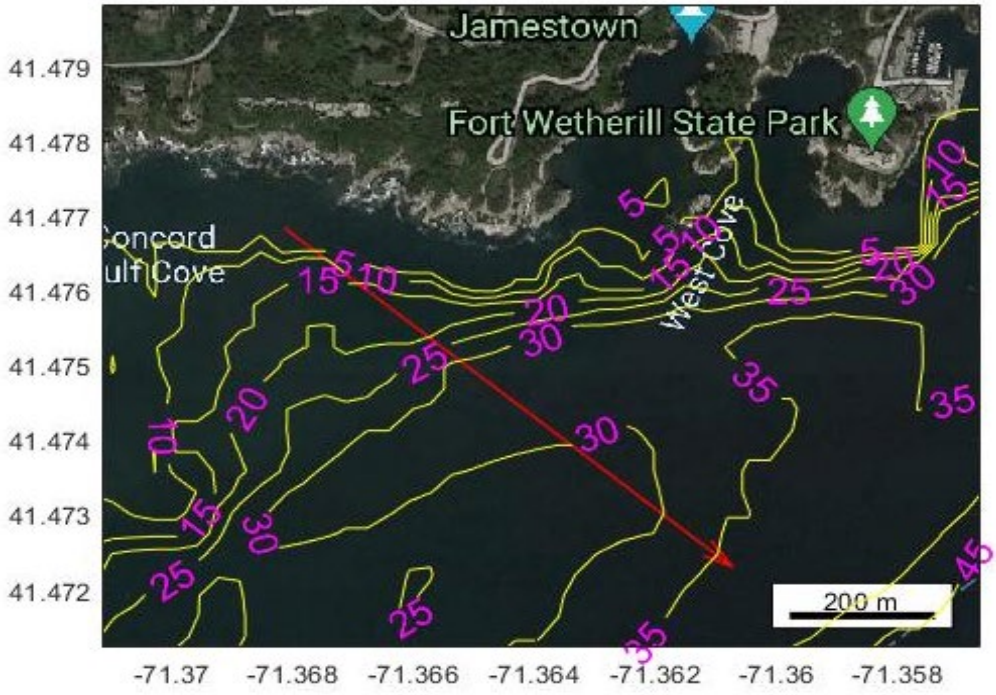

Figure 30: East Passage GPS track line and direction of drift from range testing (05/06/21) with bathymetry contours overlayed (meters).

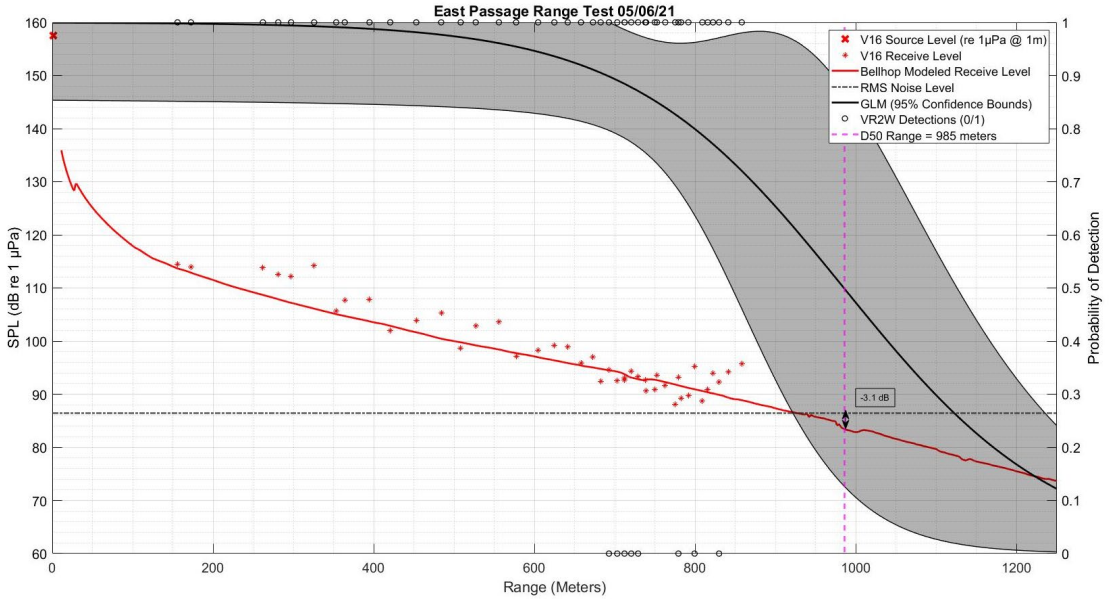

Figure 31: SPL of Vemco V16 test tags as a function of range for West Passage range test (05/06/21). GLM logistic regression for VR2W detections vs. non-detections showing probability of detection with range. Difference between Bellhop model level and RMS noise level is shown at D_{50} range.

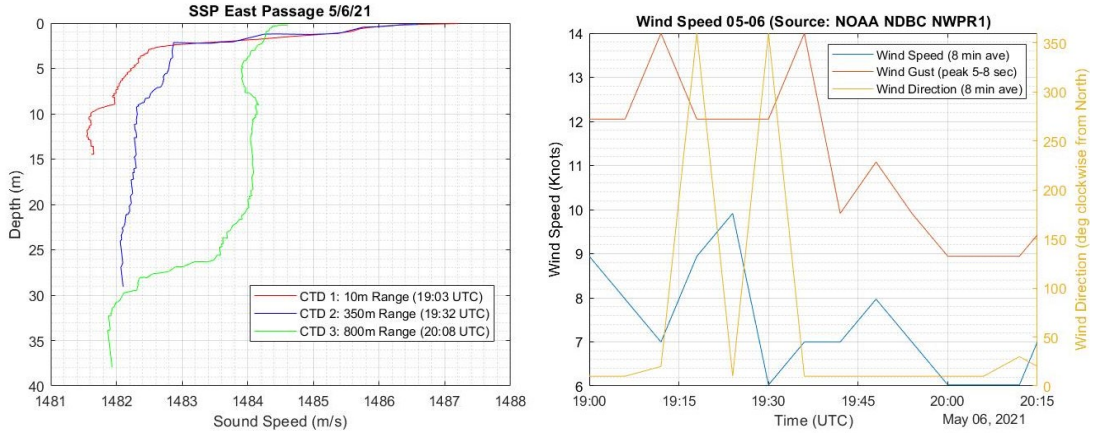

Figure 32: SSP (Left) and wind speed (Right) data for East Passage 05/06/21

4.4. Sakonnet River Data and Model

The Sakonnet River test site differed from the West and East Passage in several ways. The location is much shallower at approximately 7 meters in depth (Figure

32), and the sediment is comprised predominantly of silt. On 06/23/21 the $\boldsymbol{D_{50GLM}}$ detection range was 767 meters (Figure 32). At this range the Bellhop model level is approximately 7.8 dB above the RMS noise level. The $\boldsymbol{D_{50MDL}}$ detection range was 746.0 meters (2.7% error). The Sakonnet River location had a somewhat constrained detection range, which can be associated with a high RMS noise level (82 dB) and the increased effect due to bottom loss with a silty bottom (as compared to sandy bottom in the West Passage and East Passage) and downward refracting rays as the result of a significant thermocline (Figure 33). Additionally, at 7m depth, this location was the shallowest and therefore rays interact more with the seafloor as they travel with range.

Figure 33: Sakonnet River GPS track line and direction of drift from range testing (06/23/21) with bathymetry contours overlayed (meters).

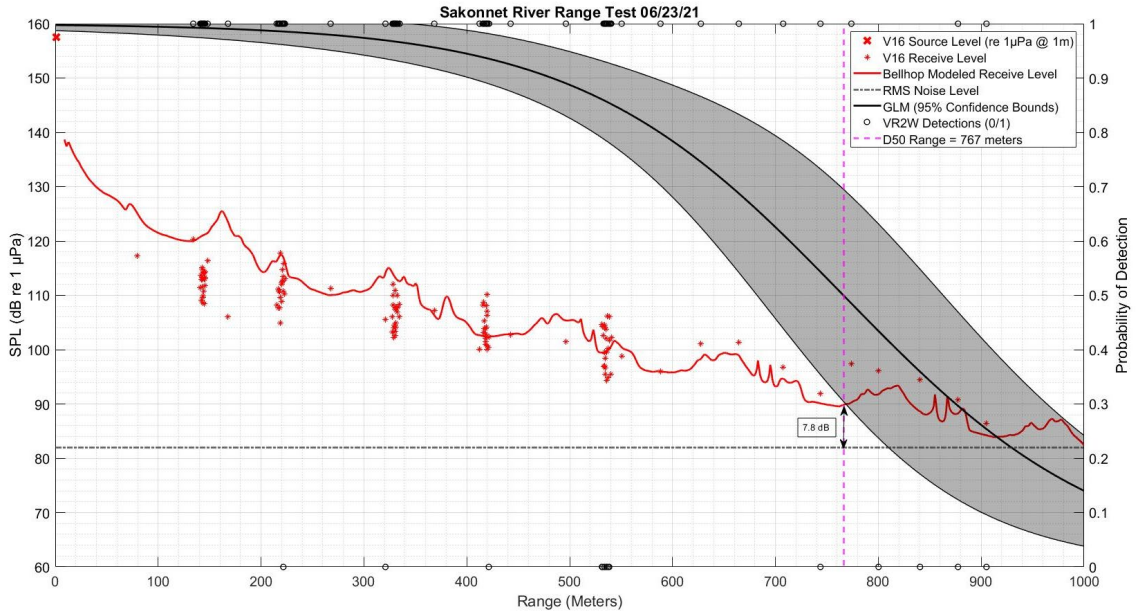

Figure 34: SPL of Vemco V16 test tags as a function of range for West Passage range test (06/23/21). GLM logistic regression for VR2W detections vs. non-detections showing probability of detection with range. Difference between Bellhop model level and RMS noise level is shown at D_{50} range.

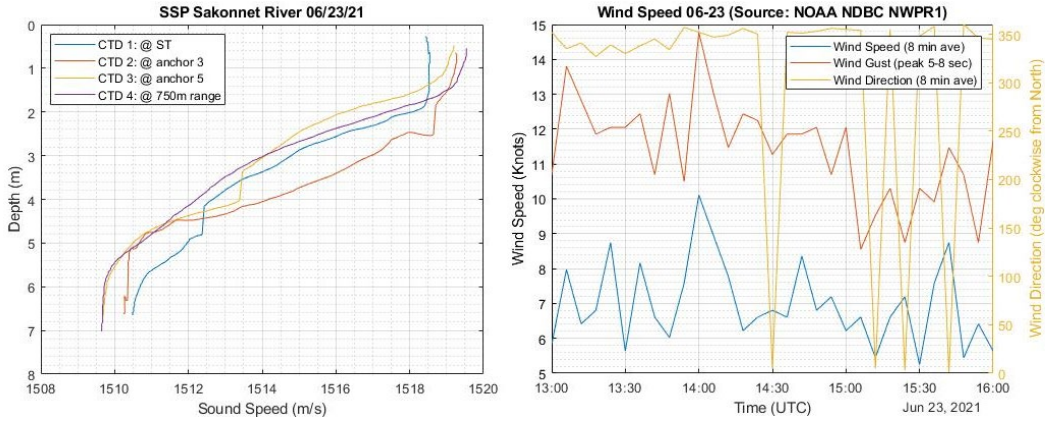

Figure 35: SSP (Left) and wind speed (Right) data for Sakonnet River 06/23/21.

4.5. Detection Matrix

Using the detection threshold (8dB above NL) established using the GLM results, a series of detection matrices utilizing hypothetical modeling scenarios in the West Passage and Block Island Sound were used to characterize the effects that

seasonal and environmental changes have on tag detection. RMS noise levels used to determine detection range ($\boldsymbol{D_{50MDL}}$) were kept constant (80 dB) for each individual matrix so that the effects of other variables (attenuation, wave bending, receiver depth) could be investigated. Each matrix shows a total of 12 scenarios which examine the effect of a receiver at the surface or bottom with sandy or silty sediment (Table 5) during Winter, Spring, and Summer SSP's (Figure 36). In the

West Passage model scenario (Table 12), detection range at the sea surface and at the bottom with a silty sediment decreased by 70-80 meters in both the winter and spring profiles, and 130-145 meters in the summer profile when compared to a sandy bottom. The increased loss in the summer profile with a silty sediment can be associated with seafloor absorption characteristics. With rays being downward refracting in the summer they encounter the seafloor more often. The difference between receivers at the surface (1m) vs at depth (10m) is not as significant. Throughout all seasons a 20–40-meter decrease in detection range is observed at surface receivers, with the spring profile observing the greatest change. The greatest detection range is in the spring and summer months with a sandy bottom and receivers at depth. This reflects the results observed by Obrien and Secor (2021) [2] that a source and receiver both placed below the thermocline can increase detection range. Overall, the West Passage location (water depth = 15m) is impacted more by bottom losses due to absorption (sediment type) rather than receiver depth.

Table 11: Matrix for West Passage model site showing $\boldsymbol{D_{50MDL}}$ detection ranges for several environmental conditions. $\boldsymbol{D_{50MDL}}$ is inferred where tag SPL is 8 dB above RMS noise level (80 dB).

50% Prob. of Detection Rng.	Winter Profile	Spring Profile	Summer Profile
Rcvr. @ Surface/ Sand Bottom	898.75m	907.50m	955.00m
Rcvr. @ Depth/ Sand Bottom	918.75m	930.00m	971.25m
Rcvr. @ Surface/ Silt Bottom	826.25m	830.00m	810.00m
Rcvr. @ Depth/ Silt Bottom	850.00m	868.75m	840.00m

Results in the Block Island model scenario (Table 13) show decreased detection range for the sandy vs silty bottom scenarios like what was seen for the West Passage scenario. The winter and spring profiles show 60–90-meter decreases in range with respect to changing sediments and the summer profile with receivers located at the depth show a 30-meter decrease in range while the summer profile with a receiver at the surface shows shows a 120-meter decrease in range (sandy vs. silty). The Block Island scenario does however show a more significant decrease in detection range with changing receiver depths of 1 and 25-meters. The winter profile sees a 45–55-meter decrease, the spring sees a 20-40-meter, and the summer sees a 50–140-meter decrease in detection ranges (receiver @ depth vs. @ surface). The Block Island location (30m depth) is impacted by both bottom losses and receiver depth, with the impact of receiver depth and bottom losses being compounded to its greatest extent in the summer profile (713-meter minimum detection range). The spring profile (March) with a

sandy bottom shows the greatest detection ranges due to very low sound speeds, minimal thermocline, and lower seafloor attenuation levels.

Table 12: Matrix for Block Island model site showing $\boldsymbol{D_{50MDL}}$ detection ranges for several environmental conditions. $\boldsymbol{D_{50MDL}}$ is inferred where tag SPL is 8 dB above RMS noise level (80 dB).

50% Prob. of Detection Rng.	Winter Profile	Spring Profile	Summer Profile
Rcvr. @ Surface/ Sand Bottom	877.50m	998.75m	835.00m
Rcvr. @ Depth/ Sand Bottom	918.75m	1017.50m	882.50m
Rcvr. @ Surface/ Silt Bottom	808.75m	908.75m	713.75m
Rcvr. @ Depth/ Silt Bottom	861.25m	948.75m	852.50m

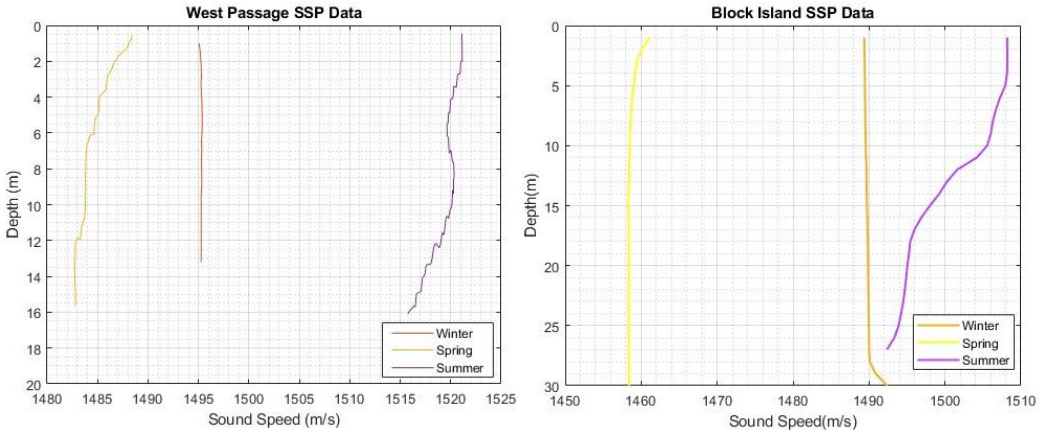

Figure 36: Winter, Spring, and Summer SSP's for West Passage (Left) and Block Island (Right) detection matrices.

CHAPTER 5

CONCLUSION

5.1. Major Findings

Predicted results using the Bellhop ray tracing program matched measured results with an accuracy of <5% percent error (Not including East Passage test due to poor GLM data). Detection ranges at 50% probability were inferred where modeled results were 8 dB above recorded RMS noise levels. Model results revealed that decreased detection ranges were associated with increased bottom losses, especially in downward refracting environments (summer thermoclines). Using worst case conditions, receiver spacing in Narragansett Bay should be adjusted to ensure that choke points in the bay are adequately covered. The lowest detection range in this study ($\boldsymbol{D_{50MDL}}$) was 690 meters, therefore at 1380 meters spacing between receivers it can be expected that all fish moving past the array will be detected. Note, however, that this range was modeled with an RMS noise level recorded during a sea state of 2-3 and scenarios with higher NL because of greater sea states were not modeled in this study. To get a true grasp of worst-case conditions, long term ambient noise studies or estimations of increased noise levels using empirical models would need to be examined. Effects due to varying receiver depth were minimal in shallow water locations, however they were more substantial in deeper water locations with significant thermoclines. Sources and receivers located below thermoclines were found to increase detection range, confirming the findings of Obrien and Secor [2]. With

these findings, caution should be taken when designing receiver arrays near the sea surface. Additionally, the bottom sediment type should be accounted for when constructing arrays, as environments with silty sediments will experience greater loss than those with sandy seafloors. With these results fisheries' management programs can make more informed decisions pertaining to receiver array construction, the uncertainty in their data, and ultimately on inferring the spatial/temporal distributions of marine species. These results will assist fisheries management programs increase the confidence of determining whether a fish was present (or detected) in lieu of other standard fishery sampling techniques (i.e., trawls, gill nets, etc.) and provides guidelines for altering receiver array design during changing seasons.

5.2. Limitations and Sources of Error

Equipment availability, vessel scheduling, and adverse weather conditions were all constant hurdles during this project. Covid-19 delays severely impacted the delivery of the Ocean Acoustics Soundtrap used in this study and at many times prevented field work from occurring. The DEM CTD was also unavailable after being sent for calibration and maintenance, forcing us to borrow CTD's of opportunity from colleagues. The 22ft Eastern motor vessel used for range testing was scheduled for other work or decommissioned for the season in the late winter. On several occasions adverse weather conditions and small boat advisories prevented field days from occurring or cut them short. Each of these factors limited the amount of range testing that could be performed during this project. Ideally, more testing would have been done for the East Passage and

Sakonnet River locations, and the GLM fits would have been better informed with a greater sample size of detections/non-detections.

One drawback to methods used was the increasing probability that transmission peaks would interfere with noise levels as transmission loss increases with range. This led to a bias in peak transmission levels when transmission loss intersected with average RMS noise levels. Model error calculations were impacted by this bias significantly for several of the range tests. Another source of error is the potential bias in calculations of RMS noise itself. Noise levels during testing days with increased ship traffic were significantly higher than those without any traffic. Additionally, self-noise from the vessel engine being turned for brief periods to retrieve anchor lines could have biased the noise calculations. The East Passage range test noise levels in this study may have been biased significantly higher than the noise levels measured in the other tests as ship traffic is quite heavy in the area. The East Passage receiver location is also quite close in proximity to a rock/cliff shoreline with breaking waves which could have also increased noise levels. These transient events likely have less of an impact on overall detectability than the bias for RMS noise level shows.

5.3. Future Considerations

While consideration was taken to diversify the locations of range testing sites, there is still uncertainty pertaining to model validity regarding adverse environments with range dependent sound speed profiles, complex bathymetries,

rough sea states, higher turbidity, increased current, etc. The Bellhop program can include the range dependent parameters of sound speed, bathymetry, altimetry, and absorption in various input files. Inclusion of these parameters could increase model accuracy and further justify the use of acoustic modeling as a tool for determining tag detectability during worst case conditions. Additionally, since Bellhop is not computationally intensive, thousands of scenarios can be run with varying environmental and design parameters. This provides researchers with the tools to create empirical models that predict detection range dependent on various parameters.

The RMS noise levels calculated during this study can show bias with regards to high transient noise levels. Work should be done to investigate whether RMS noise levels are the best representation of the noise floor for high frequency fish tag receivers. The median noise level is an alternative measurement that is not sensitive to high level transient sounds and may be better suited for estimating the ambient noise floor for the high frequency 69 kHz spectrum. It is also imperative that scientists can estimate noise levels for varying environmental conditions to avoid the need for long term statistical range testing studies. While methods for estimating ambient noise levels exist, they typically refer to the median or 50^{th} percentile of noise present in a signal and not the RMS level. Empirical formulas [1] currently used to estimate noise levels could be adjusted to predict levels closer to the noise floor and a study could be done to develop a parameter for noise level akin to the significant wave height (the average

measurement of the top 1/3rd of waves) used in hurricane and storm surge modeling.

Finally, if this testing was repeated there would have been more of an emphasis on anchoring and the range of drifts would have persisted to 1500 meters to inform the GLM with more detections/non-detections. The confidence intervals for the GLM on many of the testing days showed variability of 100-250 meters for D50 range. If the accuracy of the GLM can be improved, then the detection threshold level will be better informed.

List of References

[1] John A. Hildebrand, Kaitlin E. Frasier, Simone Baumann-Pickering, and Sean M. Wiggins , "An empirical model for wind-generated ocean noise", The Journal of the Acoustical Society of America 149, 4516-4533 (2021) https://doi.org/10.1121/10.0005430

[2] O'Brien, M.H.P., Secor, D.H. Influence of thermal stratification and storms on acoustic telemetry detection efficiency: a year-long test in the US Southern Mid-Atlantic Bight. Anim Biotelemetry 9, 8 (2021). https://doi.org/10.1186/s40317-021-00233-3

APPENDICES

Appendix A: MATLAB Functions/Scripts

```
clc; clear all; close all;
```

Specify Soundtrap filename

```
tic
filename = '5777.201119103847'; % Soundtrap file handle
disp(['Soundtrap File: ', filename])
```

XML read sample start/stop time

```
STxml = xml2struct(filename + ".log.xml");
SampleStartTimeUTC =
append(STxml.ST.PROCu_EVENT{1,2}.WavFileHandler.Attributes.SamplingStartTimeUTC,'.000');
SampleStopTimeUTC =
append(STxml.ST.PROCu_EVENT{1,4}.WavFileHandler.Attributes.SamplingStopTimeUTC,'.000');
t1 = datenum(SampleStartTimeUTC,'yyyy-mm-ddTHH:MM:SS.FFF'); % sampling start time (ms)
t2 = datenum(SampleStopTimeUTC,'yyyy-mm-ddTHH:MM:SS.FFF'); % sampling stop time (ms)
disp(['Sampling Start: ', SampleStartTimeUTC])
disp(['Sampling Stop: ', SampleStopTimeUTC])
```

Convert .wav data to units of µPa using end-end calibration value (from Soundtrap manual)

```
disp('Reading/Converting data to units of µPa...')
[y, Fs] = audioread(filename + ".wav") ; % read wav data from file
cal = 173.3; % value from calibration sheet
cal = power(10, cal / 20); % convert calibration from dB into ratio
y = y * cal; % multiply wav data by calibration to convert to units of uPa
```

Demodulate

```
disp('Demodulating Data...')
Fc = 69000; % Carrier Frequency (Hz)
[X1,X2] = demod(y,Fc,Fs,'qam'); % Quadrature demodulation
```

Decimate

```
disp('Decimating Data...')
X1 = decimate(X1,12); X1 = decimate(X1,2); % Decimate real part by factor of 24 (12 and
2)
X2 = decimate(X2,12); X2 = decimate(X2,2); % Decimate imaginary part by factor of 24 (12
and 2)
```

Low Pass Filter

```
disp('Applying Low Pass Filter...')
Fstop = 2000;                   % Cut off frequency in Hz
Wn = ((Fs/24)/2);               % Normalized freq Wn
[b,a] = butter(6,Fstop/Wn);     % Butterworth low pass filter
X1 = filtfilt(b,a,X1);          % filtfilt zero phase shift
X2 = filtfilt(b,a,X2);          % filtfilt zero phase shift
```

Compute Magnitude and Phase

```
disp('Computing Magnitude/Phase...')
XM = sqrt(X1.^2+X2.^2); % Magintude
XP = atan2(X2,X1); % Phase
```

Create datetime vector with first/last ping interval

```
disp('Creating decimated Datetime vector...')
t_num = linspace(t1,t2,length(y)); % create time vector from start time to stop time
t = datetime(t_num,'ConvertFrom','datenum'); % create datetime vector
```

Save Variables

```
disp(['Saving variables to ', filename,'.mat'])
save([filename,'.mat'],'XM','t','SampleStartTimeUTC','SampleStopTimeUTC')
toc
```

Contencate vectors from same day

```
XM = [x1.XM; x2.XM(2:end); x3.XM(2:end)];
t = [x1.t x2.t(2:end) x3.t(2:end)];
SampleStartTimeUTC = x1.SampleStartTimeUTC;
SampleStopTimeUTC = x3.SampleStopTimeUTC;
save('sk_june','XM','t','SampleStartTimeUTC', 'SampleStopTimeUTC')
```

Published with MATLAB® R2021a

Listing 1: MATLAB script for processing Soundtrap drift data.

```
clc; clear all; close all;
```

Specify test name, filename, control receiver, ST location, test tags used

```
test_name = 'West Passage 08/04/21';
filename = 'wp_august'; load([filename,'.mat']) % Load ST processed data file
control_receiver = r135471;     % r134922 (control), r135470 (bottom), r135472 (top)
ST_location = [gps_waypoints.Latitude(3),gps_waypoints.Longitude(3)]; % Soundtrap GPS
location
tag = ["A69-1602-59951"];       % A69-1602-59950/1 (Lo/Hi/7m), A69-1602-21114/5
(Lo/Hi/3m)
```

Automate Transmission Peak Averaging

```
tic
% Find control receiver ping time index (make sure Vemco file is trimmed accordingly!)
PingTimeIndex = find(control_receiver.time >= SampleStartTimeUTC & control_receiver.time
<= SampleStopTimeUTC);
PingTagIndex = PingTimeIndex(find(control_receiver.tag(PingTimeIndex) == tag)); % Find
which tag occurred at each PingTimeIndex

clear peak_mean loc_mean
for i = 1:length(PingTagIndex)-1
    % Determine ping index
    ti = find(t >= control_receiver.time(PingTagIndex(i))- seconds(2.5) t <=
control_receiver.time(PingTagIndex(i))+ seconds(2.5)); % (+- 2.5 Hi pwr 11/19)

    % Find peaks of transmission
    [peaks, locs] = findpeaks(XM(ti),
t(ti),'MinPeakHeight',1e4,'MinPeakDistance',seconds(.25),'NPeaks',8,'SortStr','descend');
    peak_mean(i) = mean(peaks); % Calculate mean pressure level of ping peaks
    loc_mean(i) = mean(locs); % Calculate mean of ping peak times
    error(i) = std(peaks); % Compute standard deviation of peaks

%         % Plot demod/dec ST data interval
%         figure(i+1)
%         plot(t(ti),XM(ti)); hold on      % Demod/dec ST data
%         plot(locs, peaks, '*')  % Plot peaks of transmissions
%
%         % Format plot
%         xlabel('Time (UTC)'); ylabel('Pressure (µPa)');title("Demodulated/Decimated ST
Data "+ test_name)
%         set(gca,'FontSize',15) % Sets FontSize to 15
%         legend('Soundtrap')
%         grid on; grid minor;
%
%         % Plot line for receiver time
%
xline(control_receiver.time(PingTagIndex(i)),'r','LineWidth',2,'DisplayName','A69-1602-
59951 (Hi/7m)')

end

% Compute Range for pings using GPS track
gps_time = datenum(gps_track.Time, 'yyyy-mm-ddTHH:MM:SS'); % Convert gps time string to
datenum vector
gps_time = datetime(gps_time,'ConvertFrom','datenum'); % Convert gps datenum to datetime
vector
SPL = 20*log10(peak_mean); % Convert Pressure (uPa) to SPL (dB)

clear range closest_index
for i = 1:length(loc_mean)
    target = loc_mean(i); % Target value.
    temp = abs(target - gps_time); % Temporary "distances" array.
    closest_index(i) = find(temp == min(abs(target - gps_time))); % Find "closest" values
array wrt. target value.
    range(i) =
deg2km(distance(ST_location(1),ST_location(2),gps_track.Latitude(closest_index(i)),gps_tr
ack.Longitude(closest_index(i))))*1000; % Compute range (m) from hydrophone to ping
end

% Circle pings that werent detected
r135470.detections = []; r135472.detections = [];
for i = 1:length(loc_mean)
    if any(r135470.time >= loc_mean(i)-seconds(2.5) & r135470.time <=
loc_mean(i)+seconds(2.5))
        r135470.detections(i) = 1;
    else
        r135470.detections(i) = 0;
```

```
    end

    if any(r135472.time >= loc_mean(i)-seconds(2.5) & r135472.time <=
loc_mean(i)+seconds(2.5))
        r135472.detections(i) = 1;
    else
        r135472.detections(i) = 0;
    end
end

% Plot SPL, rms noise, non-detections vs Range
figure
plot(range,SPL, 'r*'); hold on
plot(range(find(r135470.detections == 0)), SPL(find(r135470.detections == 0)), 'ko',
'MarkerSize', 10)
plot(range(find(r135472.detections == 0)), SPL(find(r135472.detections == 0)), 'kx',
'MarkerSize', 10)

toc

% Plot SL of Hi Power Pings
plot(1,157.5,'rx','MarkerSize',10,'LineWidth',3) % Plot SL of Hi Pingers @ 1m
```

Format Plot

```
xlabel('Range(m)'); ylabel('SPL (dB re 1 µPa)'); title("SPL vs Range: " + test_name)
ylim([65 160])
set(gca,'FontSize',15) % Sets FontSize to 15
grid on; grid minor;
legend('Hi Power Average (Tag 7m depth)', 'NOT DETECTED (VR2W 10m depth)','NOT DETECTED
(VR2W 10m depth)', 'Hi SL (157.5 dB re 1 µPa)')
```

Plot Prob of Detection vs Range

West Passage May

```
wp_may.range = [345 520 620 710 810];
wp_may.prob_bottom = [.96 .92 .86 .80 .55];
wp_may.prob_top = [1 1 .95 .85 .73];
% Sakonnet June
sr_jun.range = [130 204 315 404 522];
sr_jun.prob_bottom = [1 1 .95 .96 .74];
sr_jun.prob_top = [1 .95 .95 .91 .65];
% West Passage August
wp_aug.range = [305 400 550 750 915];
wp_aug.prob_bottom = [1 1 .74 .15 0];
wp_aug.prob_top = [1 1 .87 .30 .18];

% Plot on right y axis
yyaxis right
ylim([0 1])
plot(wp_may.range, wp_may.prob_bottom,'DisplayName','Detection Probability (VR2W 10m
depth)')
plot(wp_may.range, wp_may.prob_top,'DisplayName','Detection Probability (VR2W 6m depth)')
```

Compute RMS noise entire drift

```
XM_rms = 20*log10(sqrt(mean(XM(find(t >= r135471.time(1),1):find(t >=
r135471.time(end),1)).^2))); % 08-04 ep
XM_median = 20*log10(median(XM(find(t >= r135471.time(1),1):find(t >=
r135471.time(end),1)))); % 08-04 ep
yline(XM_rms,'DisplayName', 'RMS Noise Level (entire drift)')
%yline(XM_median,'DisplayName', 'Median Noise Level (entire drift)')
```

Compute MAPE (Mean Abs Percent Error) for model

Published with MATLAB® R2021a

Listing 2: Script for transmission peak averaging and plotting of SPL vs Range.

```
function [ctd] = read_ysi(filename)
%[ctd] = read_ysi(filename)
%
%   Read YSI .csv file and create ctd object. Compute SSP with
%   medwin(T,S,z) function. ctd object includes Temperature (C), Salinity
%   (ppt), depth (m), and pH (0-14).
```

Load CTD data from YSI device (.csv file)

```
ctd.data = readmatrix(filename,'Range','B:N');
ctd.time = readmatrix(filename,'OutputType', 'char',
'ExpectedNumVariables',1,'DateLocale','en_US');
ctd.time = datetime(ctd.time,'InputFormat','MM/dd/yy HH:mm:ss', 'TimeZone','local');
ctd.time.TimeZone = 'Z'; % Convert to UTC time
```

Read variables from YSI CTD data

```
ctd.T = ctd.data(:,1); % Temperature (C)
ctd.S = ctd.data(:,3); % Salinity (ppt)
ctd.z = ctd.data(:,4); % Depth (m)
ctd.pH = ctd.data(:,5); % pH (0-14)
```

Compute SSP from data using Medwins Eq

```
ctd.c = medwin(ctd.T,ctd.S,ctd.z); % SSP (m/s)
```

Plot SSP, T, S, pH Profiles

```
figure;
plot(ctd.c,ctd.z); xlabel('Sound Speed (m/s)'); axis ij; grid minor; ylabel('Depth (m)');
title('SSP');
figure;
subplot(1,4,1); plot(ctd.c,ctd.z); xlabel('Sound Speed (m/s)'); axis ij; grid minor;
ylabel('Depth (m)');
subplot(1,4,2); plot(ctd.T,ctd.z); xlabel('Temperature (C)'); axis ij; grid minor;
ylabel('Depth (m)');
subplot(1,4,3); plot(ctd.S,ctd.z); xlabel('Salinity (ppt)'); axis ij; grid minor;
ylabel('Depth (m)');
subplot(1,4,4); plot(ctd.pH,ctd.z); xlabel('pH (0-14)'); axis ij; grid minor;
ylabel('Depth (m)');
sgtitle('Sound Speed, Temperature, Salinity, and pH Profiles');
end
```

Published with MATLAB® R2021a

Listing 3: MATLAB script for reading/plotting YSI Sonde CTD data.

```
function [alpha_AM] = absorption_AM( f, S, T, pH, z )

% [alpha_AM] = absorption_AM( f, S, T, pH, z )
%
%   Francois-Garrison/Ainslie-McColm attenuation.
%   See Ainslie and McColm, JASA 103(3):1671- 1998
%
%   Input: (f(kHz), S(ppt), T(C), pH(0-14), z(m))
%   Output: absorption (dB/km); for Bellhop convert to dB/wavelength
%
%   IF NO PH LEVELS USE DEFAULT OF PH=8

% Ainslie-McColm
f1 = 0.78 .* sqrt( S./ 35 ) .* exp( T./ 26 );   % boron
f2 = 42 .* exp( T./ 17 );   % magnesium
alpha_AM = 0.106 .* f1 .* f.^2 ./ ( f.^2 + f1.^2 ) .* exp( ( pH - 8 ) / 0.56 ) + ...
    + 0.52 .* ( 1 + T./ 43 ) .* ( S./ 35 ) .* f2 .* f.^2 ./ ( f.^2 + f2.^2 ) .* exp( (-
z./1000)./ 6 ) + ...
    + 0.00049 .* f.^2 .* exp( - ( T./27 + (z./1000)./ 17 ) );
end
```

Published with MATLAB® R2021a

Listing 4: MATLAB function for computing Ainslie-McColm absorption.

```
function [alpha_KF] = absorption_KF( f, T, z )

% [alpha_KF] = absorption_KF( f, T, z )
%
%   Kinsler-Frey attenuation w/ temperature (°C) valid range: 0 <= T_C <= 30
%   hydrostatic pressure (atm) valid range: 1 <= P_atm <= 400
%   See: Kinsler, Frey, Coppens, and Sanders. Fundamentals of
%   Acoustics, 3rd Ed.  Pages 158 through 160.  Model reprinted from
%   Fisher and Simmons.  J. Acoust. Soc. Am 62, 558, 1976
%
%   Input: (f(kHz), T(C), z(m))
%   Output: absorption (dB/km); for Bellhop convert to dB/wavelength


% Kinsler/Frey
P = (z.*1025.*9.81)./101325;
f1 = 1320.*(T + 273.15).*exp(-1700./(T + 273.15));
f2 = (1.55e+7).*(T + 273.15).*exp(-3052./(T + 273.15));
```

```
A = (8.95e-8).*(1 + .023.*T - (5.1e-4).*T.^2);
B = (4.88e-7).*(1 + .013.*T).*(1 - (.9e-3).*P);
C = (4.76e-13).*(1 - .04.*T + (5.9e-4).*T.^2).*(1 - (3.8e-4).*P);
alpha_KF = ((A.*f1.*((f*1000).^2))./(f1.^2 + (f*1000).^2) +...
    (B.*f2.*((f*1000).^2))./(f2.^2 + (f*1000).^2) +...
    C.*((f*1000).^2))*1000;
end
```

Published with MATLAB® R2021a

Listing 5: Function for computing Kinsler-Frey absorption.

```
function [c] = medwin(T,S,z)

% [c] = medwin(T,S,z)
%
%   Medwin's Equation for SSP w inputs (T,S,z), Temperature (C),
%   Salinity (ppt), and Depth (m). Output c (m/s).

c = 1449.2+4.6.*T-(5.5*10^(-2)).*T.^2+(2.9*10^(-4)).*T.^3+(1.34-10^(-2).*T).*(S-
35)+(1.6*10^(-2)).*z;
end
```

Published with MATLAB® R2021a

Listing 6: MATLAB function for computing sound speed using the Medwin equation.

```
%--------------------%

%  RIDEM DMF/URI
%  Bellhop Modeling
%  4/27/21
%--------------------%

clc; clear all; close all;
```

Filename

```
filename = 'sakonnet_06-23';
```

Plot Model SSP

```
figure
plotssp(filename + ".env")
title('SSP')
grid on;
```

Bellhop Rays

```
figure
bellhop(filename) % Change env file to 'R' case (ray)
plotray(filename)
```

Bellhop shd + TL

```
bellhop(filename) % Change env file to 'IB' case (incoherent TL, Gaussian Beam)
figure
plotshd(append(filename, '.shd'), 69000)
figure
[rkm_incoherent, tl_incoherent] = plottlr(append(filename, '.shd'),4);
grid on; grid minor;
```

Save variables

```
save('TL_sr_june','rkm_incoherent','tl_incoherent')
```

Plot tlr Hi pwr SL

```
plot(rkm_incoherent(6:end)*1000,157.5-tl_incoherent(6:end),'r-','DisplayName','Hi Power
Model')
xlim([0 1200])
```

Published with MATLAB® R2021a

Listing 7: MATLAB script to run Bellhop program.

```
clc; clear all; close all;
```

Logistic Regression Analysis

```
d = readtable('GLM_data_matlab.xlsx','ReadRowNames',true,"UseExcel",true)
y = d.Detection;
X = d.Range;
test = d.Test;
```

Plot Regression and Confidence Intervals Splice plot

```
range_test = 2;% 1=wp_nov17, 2=wp_nov19, 3=wp_may06, 4=ep_may06, 5=sr_jun23, 6=wp_aug04
index = find(test == range_test);
glm_data = sortrows([X(index) y(index)]);
mdl = fitglm(glm_data(:,1),glm_data(:,2),'linear','Distribution','binomial')
plotSlice(mdl)
```

Plot GLM fit

```
colororder({'k','k'})
yyaxis right
[b,dev,stats] = glmfit(glm_data(:,1),glm_data(:,2),'binomial','Link','logit');
range_vector = linspace(0,1250,1250);
[yfit, dylo, dyhi] = glmval(b,range_vector,'logit',stats);

% Plot GLM fit
h_glm = plot(range_vector,yfit,'k-','LineWidth',2,'DisplayName','GLM (95% Confidence
Bounds)')

% Plot detections
plot(glm_data(:,1),glm_data(:,2),'ko','LineWidth',1,'DisplayName','VR2W Detections
(0/1)')

% Plot 95% confidence bounds
err_lo = yfit-dylo;
err_hi = yfit+dylo;
%plot(range_vector,err_lo,'k--',range_vector,err_hi,'k--')
h = shade(range_vector,err_lo,'k-',range_vector,err_hi,'k-','FillType',[2
1],'LineWidth',1,'Marker','none');

% Format
ylim([0 1]);
ylabel('Probability of Detection')
```

Plot and calculate d50 range

Calculate Detection threshold level

```
d50modelrange_lo = find(rkm_incoherent*1000 >= d50_lo,1);
d50modelrange_hi = find(rkm_incoherent*1000 >= d50_hi,1);
d50modelrange = find(rkm_incoherent*1000 >= d50,1);

d50threshold_lo = 157.5-tl_incoherent(d50modelrange_lo)- XM_rms;
d50threshold_hi = 157.5-tl_incoherent(d50modelrange_hi)- XM_rms;
d50threshold = 157.5-tl_incoherent(d50modelrange)- XM_rms
```

Calculate Detection Threshold Range w/ Bellhop Output and NL

```
threshold = 8; % dB above NL
tl_incoherent_trim = tl_incoherent(20:end);
rkm_incoherent_trim = rkm_incoherent(20:end);
bhop_range = rkm_incoherent_trim(find(tl_incoherent_trim >= (157.5 - XM_rms -
threshold),1))*1000
```

Plot detection threshold and bhop range

```
detection_threshold = XM_rms + threshold;
yline(detection_threshold,'g','DisplayName','Detection Threshold (8 dB >
NL)','LineWidth',2)
```

Plot GLM fit all locations

```
plot(linspace(0,1250,1250),yfit,'c-','LineWidth',2)
legend('West Passage 11/17/21','West Passage 11/19/21','West Passage 05/06/21','East
Passage 05/06/21','Sakonnet River 06/23/21','West Passage 08/04/21','d50 Probability')
```

Published with MATLAB® R2021a

Listing 8: MATLAB script to run GLM logistic regression.

Appendix B: Detection Matrix Modeling Scenarios

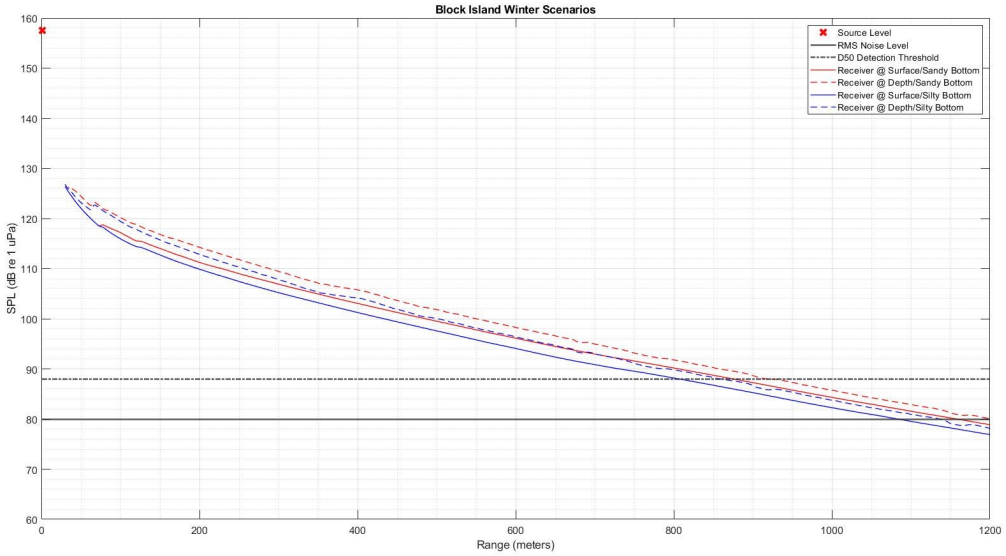

Figure 37: Block Island Winter matrix scenarios.

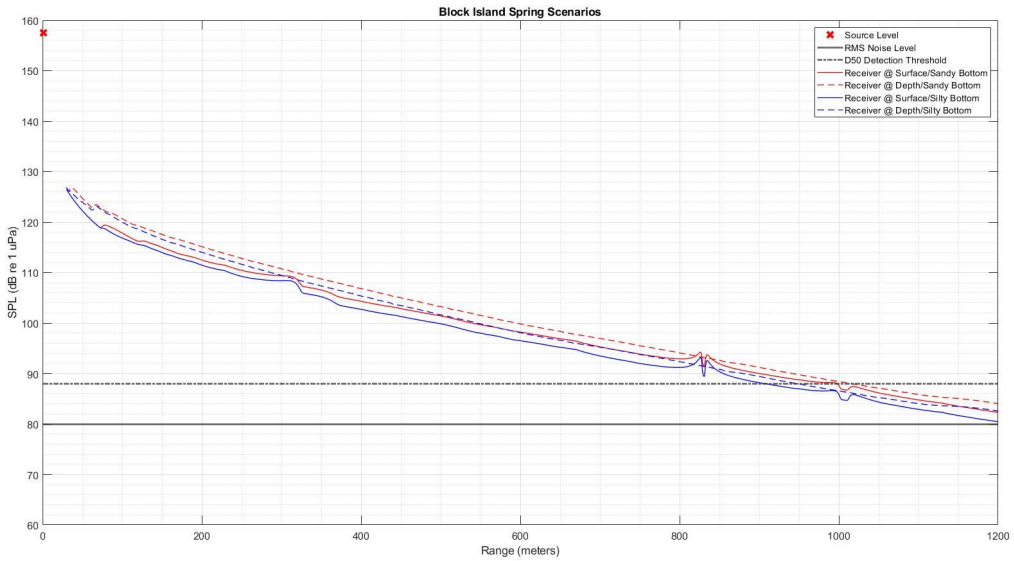

Figure 38: Block Island spring detection matrix scenarios.

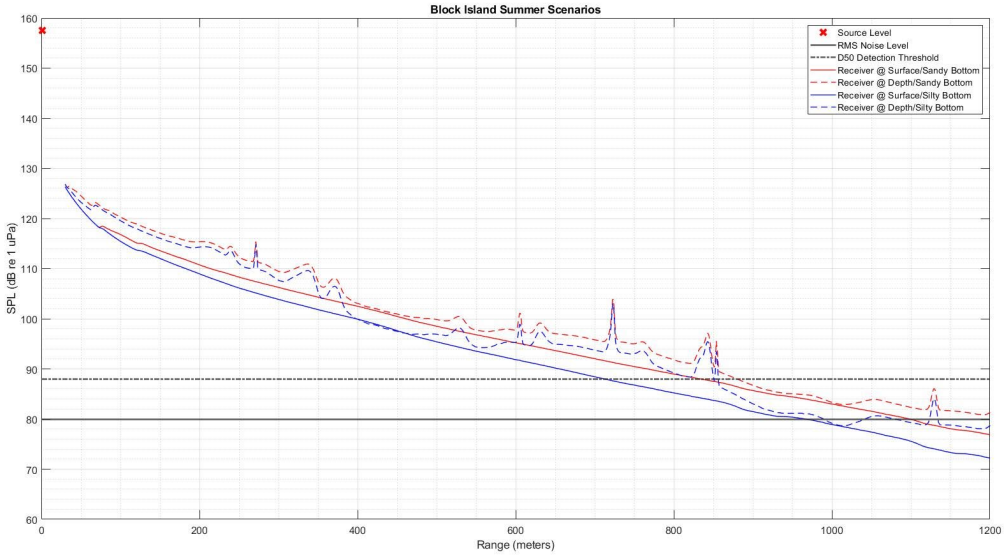

Figure 39: Block Island Summer detection matrix scenarios.

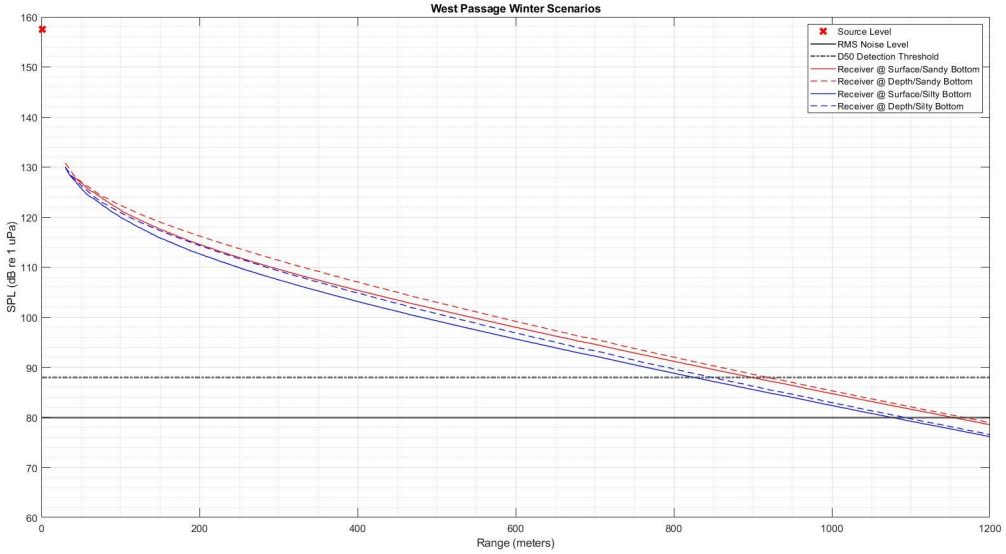

Figure 40: West Passage winter matrix scenarios.

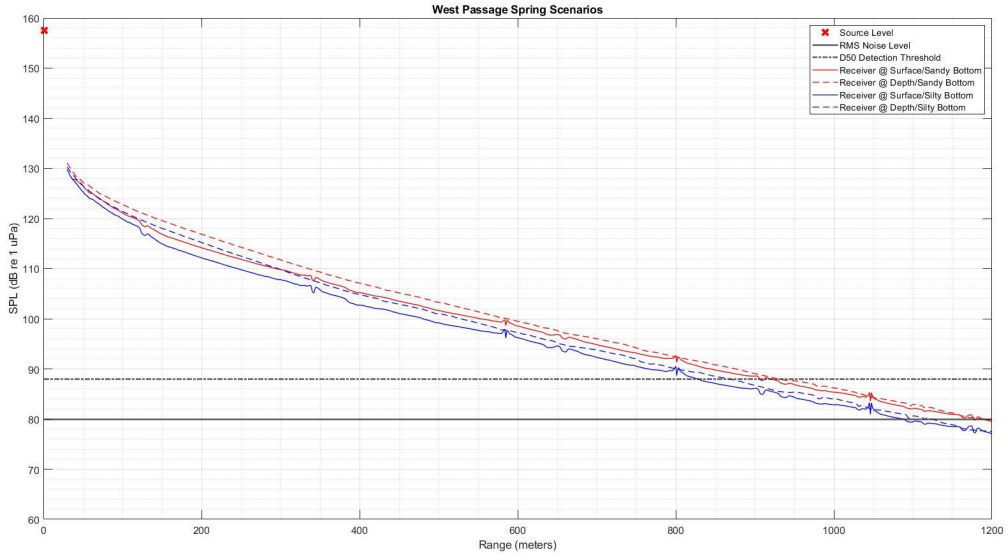

Figure 41: West Passage spring detection matrix scenarios.

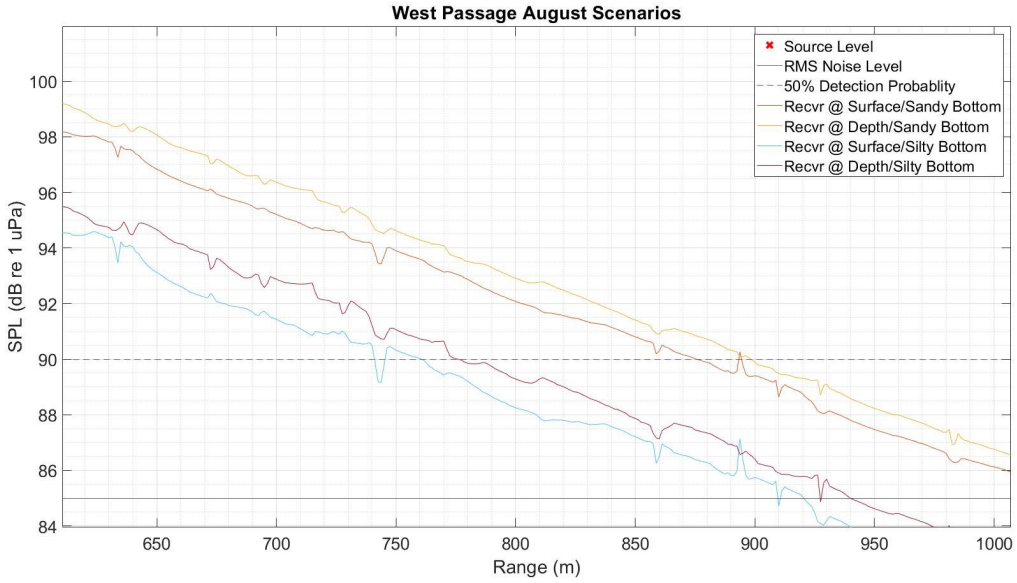

Figure 42: West Passage Summer detection matrix scenarios.

BIBLIOGRAPHY

ACT (Atlantic Cooperative Telemetry) Network. 2020. The Atlantic Cooperative Telemetry Network. Available: www.theactnetwork.com. (April 2020).

Ainslie M. A., McColm J. G., "A simplified formula for viscous and chemical absorption in sea water", Journal of the Acoustical Society of America, 103(3), 1671-1672, 1998.

Atlantic States Marine Fisheries Commission (ASMFC). 2017. Atlantic Sturgeon Benchmark Stock Assessment Report for Peer Review. Stock Asses. Rep. No. XX-XX X. ASMFC, Arlington VA. 237 pp. Manuscript in peer review.

Badiey, M. (2015). Fluctuations of Broadband Acoustic Signals in Shallow Water.

Bangley, C.W., Whoriskey, F.G., Young, J.M. and Ogburn, M.B. (2020), Networked Animal Telemetry in the Northwest Atlantic and Caribbean Waters. Mar Coast Fish, 12: 339-347. https://doi.org/10.1002/mcf2.10128

Discovery of Sound in the Sea (DOSITS). Detection Threshold for Sonar – Discovery of Sound in the Sea (dosits.org)

Discovery of Sound in the Sea (DOSITS). Sonar Equation Example: Passive Sonar – Discovery of Sound in the Sea (dosits.org)

Discovery of Sound in the Sea (DOSITS). source level – Discovery of Sound in the Sea (dosits.org)

Discovery of Sound in the Sea (DOSITS). How does sound travel in shallow water? – Discovery of Sound in the Sea (dosits.org)

Douglas G. Pincock. (2009). Detection Performance of Lines of VR2W/VR3 Receivers. AMIRIX Systems Inc.

Eric Schneider. Rhode Island Marine Fisheries Institute. U.S. Fish and Wildlife State Wildlife Grant. DOCUMENTING THE SPATIAL AND TEMPORAL DISTRIBUTION OF ATLANTIC STURGEON IN RHODE ISLAND STATE WATERS (uri.edu)

Francois R. E., Garrison G. R., "Sound absorption based on ocean measurements: Part II:Boric acid contribution and equation for total absorption", Journal of the Acoustical Society of America, **72**(6), 1879-1890, 1982.

Goulette, G.S. and Hawkes, J.P. (2017), Altering Vertical Placement of Hydroacoustic Receivers for Improved Efficiency in Coldwater Estuary Zones. North American Journal of Fisheries Management, 37: 981-988. https://doi.org/10.1080/02755947.2017.1336133

Hilton, E.J., B. Kynard, M.T. Balazik, A.Z. Horodysky, and C.B. Dillman. 2017. Review of the biology, fisheries, and conservation status of the Atlantic sturgeon (Acipenser oxyrinchus oxyrinchus Mitchell, 1815). Journal of Applied Ichthyology 32 (Suppl. 1): 30-66.

Huveneers, C., Simpfendorfer, C.A., Kim, S., Semmens, J.M., Hobday, A.J., Pederson, H., Stieglitz, T., Vallee, R., Webber, D., Heupel, M.R., Peddemors, V. and Harcourt, R.G. (2016), The influence of environmental parameters on the performance and detection range of acoustic receivers. Methods Ecol Evol, 7: 825-835. https://doi.org/10.1111/2041-210X.12520

James, Gareth., Witten, Daniela., Hastie, Trevor., Tibshirani, Robert. 2014. An Introduction to Statistical Learning: With Applications in R. Springer Publishing Company, Incorporated.

James P. Kilfoil, Bradley M. Wetherbee, John K. Carlson & Dewayne A. Fox (2017) Targeted Catch-and-Release of Prohibited Sharks: Sand Tigers in Coastal Delaware Waters, Fisheries, 42:5, 281-287, DOI: 10.1080/03632415.2017.1306974

John A. Hildebrand, Kaitlin E. Frasier, Simone Baumann-Pickering, and Sean M. Wiggins , "An empirical model for wind-generated ocean noise", The Journal of the Acoustical Society of America 149, 4516-4533 (2021) https://doi.org/10.1121/10.0005430

Kessel, S.T., Cooke, S.J., Heupel, M.R. et al. A review of detection range testing in aquatic passive acoustic telemetry studies. Rev Fish Biol Fisheries 24, 199–218 (2014). https://doi.org/10.1007/s11160-013-9328-4

Kraus RT, Holbrook CM, Vandergoot CS, et al. Evaluation of acoustic telemetry grids for determining aquatic animal movement and survival. Methods Ecol Evol. 2018;00:1–14. https://doi.org/10.1111/2041-210X.12996

Kuperman, W. (1996). Acoustic Propagation Modeling in Shallow Water.

Loher, T., Webster, R.A. & Carlile, D. A test of the detection range of acoustic transmitters and receivers deployed in deep waters of Southeast Alaska, USA. Anim Biotelemetry 5, 27 (2017). https://doi.org/10.1186/s40317-017-0142-y

McMaster, Robert; Sediments of Narragansett Bay system and Rhode Island Sound, Rhode Island. Journal of Sedimentary Research 1960; 30 (2): 249–274. doi: https://doi.org/10.1306/74D70A15-2B21-11D7-8648000102C1865D

McMullen, K.Y., Poppe, L.J., Blackwood, D.S., Nardi, M.J., and Andring, M.A., 2015, Sea-floor morphology and sedimentary environments in southern

Narragansett Bay, Rhode Island: U.S. Geological Survey Open-File Report 2015–1149, 1 DVD-ROM, http://dx.doi.org/10.3133/ofr20151149.

Medwin, H, "Speed of sound in water: A simple equation for realistic parameters", The Journal of the Acoustical Society of America 58, 1318-1319 (1975) https://doi.org/10.1121/1.380790

Melnychuk, M.C., Walters, C.J. Estimating detection probabilities of tagged fish migrating past fixed receiver stations using only local information. Canadian Journal of Fisheries and Aquatic Sciences. 67(4): 641-658. https://doi.org/10.1139/F09-199

Michael A. Ainslie and James G. McColm , "A simplified formula for viscous and chemical absorption in sea water", The Journal of the Acoustical Society of America 103, 1671-1672 (1998) https://doi.org/10.1121/1.421258

Morozs, Nils; Gorma, Wael; Henson, Benjamin; Shen, Lu; Mitchell, Paul; Zakharov, Yuriy (2020): Channel Modeling for Underwater Acoustic Network Simulation. TechRxiv. Preprint. https://doi.org/10.36227/techrxiv.11958852.v1

National Research Council (U.S.) (Ed.). (2003). Ocean noise and marine mammals. Washington, D.C: National Academies Press.

O'Brien, M.H.P., Secor, D.H. Influence of thermal stratification and storms on acoustic telemetry detection efficiency: a year-long test in the US Southern Mid-Atlantic Bight. Anim Biotelemetry 9, 8 (2021). https://doi.org/10.1186/s40317-021-00233-3

Ocean Acoustics Inc. Soundtrap ST300 specification sheet. SoundTrap-300-Spec.pdf (oceaninstruments.co.nz).

Ocean Acoustics Inc. Soundtrap ST300 Manual. www.oceaninstruments.co.nz/wp-content/uploads/2015/04/ST-User-Guide.pdf

Ocean Acoustics Toolbox OALIB (oalib-acoustics.org)

Parkins. Chris. Rhode Island Department of Environmental Management Division of Marine Fisheries Acoustic Telemetry Array (RIDEM DMF). 2021.

Pincock, D. (2009). Detection Performance of Lines of VR2W/VR3 Receivers. AMIRIX Systems Inc. Vemco Division.

Porter, M. (2019). The BELLHOP Manual and User's Guide.

Porter, M. (1992). The KRAKEN normal mode program.

Pusey, Grant & Duncan, Alec & Smerdon, A.M.. (2009). Analysis of acoustic modem performance for long range horizontal data transmission. 1 - 9. 10.1109/OCEANSE.2009.5278203

Rhode Island Department of Environmental Management (RIDEM). 2015. Rhode Island State Wildlife Action Plan (RI SWAP). Available at: http://www.dem.ri.gov/programs/fish-wildlife/wildlifehuntered/swap15.php

Robinson, Stephen & Lepper, Paul & Hazelwood, Richard. (2014). Good Practice Guide No. 133 Underwater Noise Measurement. National Physical Laboratory.

Secor DH, O'Brien MHP, Gahagan BI, Watterson JC, Fox DA (2020) Differential migration in Chesapeake Bay striped bass. PLoS ONE 15(5):e0233103. https://doi.org/10.1371/journal.pone.0233103

Selby, T.H., Hart, K.M., Fujisaki, I., Smith, B.J., Pollock, C.J., Hillis-Starr, Z., Lundgren, I. and Oli, M.K. (2016), Can you hear me now? Range-testing a submerged passive acoustic receiver array in a Caribbean coral reef habitat. Ecol Evol, 6: 4823-4835. https://doi.org/10.1002/ece3.2228

Urick, R. J. (1983). Principles of Underwater Sound, Third Edition (3rd edition, Reprint 2013). New York: McGraw-Hill, Inc.

VEMCO. How do PPM coded tags work?. How do PPM coded tags work? (vemco.com)

VEMCO. How much detection range can I expect from my tags and receivers? How much detection range can I expect from my tags and receivers? (innovasea.com)

VEMCO. Acoustic Telemetry Conference Presentation. 2007. Microsoft PowerPoint - Sydney2007 [Compatibility Mode] (imos.org.au)

VEMCO. VR2W receiver specification sheet. vr2w-1.pdf (oceans-research.com).

VEMCO. V16 tag specification sheet. v16-coded-1.pdf (oceans-research.com)

Wenz, G. M. "Acoustic Ambient Noise in the Ocean: Spectra and Sources," Journal of the Acoustical Society of America, Vol. 34, No. 12, 1962, pp. 1936-1956. doi:10.1121/1.1909155

Wingate, R.L., Secor, D.H. and Kraus, R.T. (2011), Seasonal Patterns of Movement and Residency by Striped Bass within a Subestuary of the Chesapeake Bay. Transactions of the American Fisheries Society, 140: 1441-1450. https://doi.org/10.1080/00028487.2011.630279

YSI 6920 V2-2 Multiparameter Water Quality Sonde. SECTION 1 INTRODUCTION (ysi.com)

Ziomek, L. J. (1995). Fundamentals of acoustic field theory and space-time signal processing. Boca Raton: CRC Press.